AECL--10533

CA9200704

ATOMIC ENERGY OF CANADA LIMITED

ÉNERGIE ATOMIQUE DU CANADA LIMITÉE

THE ACCELERATION OF PARTICLES BY RELATIVISTIC ELECTRON PLASMA WAVES DRIVEN BY THE OPTICAL MIXING OF LASER LIGHT IN A PLASMA

ACCÉLÉRATION DE PARTICULES À L'AIDE D'ONDES DE PLASMA ÉLECTRONIQUE RELATIVISTES EXCITÉES PAR LE MÉLANGE OPTIQUE DE LUMIÈRE LASER DANS UN PLASMA

N.A. EBRAHIM and S.R. DOUGLAS

Chalk River Laboratories

Laboratoires de Chalk River

Chalk River, Ontario K0J 1J0

March 1992 mars

AECL Research

THE ACCELERATION OF PARTICLES BY RELATIVISTIC ELECTRON PLASMA WAVES DRIVEN BY THE OPTICAL MIXING OF LASER LIGHT IN A PLASMA

by

Nizar A. Ebrahim* and Stephen R. Douglas**

*Accelerator Physics Branch
**Mathematics and Computation Branch
Chalk River Laboratories
Chalk River, Ontario, Canada, K0J 1J0
1992 March

AECL-10583

EACL Recherche

ACCÉLÉRATION DE PARTICULES À L'AIDE D'ONDES DE PLASMA ÉLECTRONIQUE RELATIVISTES EXCITÉES PAR LE MÉLANGE OPTIQUE DE LUMIÈRE LASER DANS UN PLASMA

par

Nizar A. Ebrahim* et Stephen R. Douglas**

RÉSUMÉ

À l'aide d'etudes théoriques et de simulations de particules, on étudie l'accélération des électrons au moyen d'ondes de plasma électronique relativistes de grand amplitude. L'accélération maximale pouvant être obtenue grâce à ce processus est fonction d'un grand nombre de facteurs. Le présent rapport présente une étude de l'impact de ces facteurs sur le mécanisme d'accélération. Bien que l'on fasse particulièrement référence au concept d'accélérateur a onde de battement, l'étude se rapporte également à l'accélération de particules par les ondes de chocs produites dans le plasma soit par des particules ou un laser.

*Physique des accélérateurs
**Mathématiques et Calcul
Laboratoires de Chalk River
Chalk River (Ontario)
Canada K0J 1J0
Mars 1992

AECL-10583

AECL Research

THE ACCELERATION OF PARTICLES BY RELATIVISTIC ELECTRON PLASMA WAVES DRIVEN BY THE OPTICAL MIXING OF LASER LIGHT IN A PLASMA

by

Nizar A. Ebrahim* and Stephen R. Douglas**

Abstract

Electron acceleration by relativistic large-amplitude electron plasma waves is studied by theory and particle simulations. The maximum acceleration that can be obtained from this process depends on many different factors. This report presents a study of how these various factors impact on the acceleration mechanism. Although particular reference is made to the laser plasma beatwave concept, the study is equally relevant to the acceleration of particles in the plasma wakefield accelerator and the laser wakefield accelerator.

*Accelerator Physics Branch
**Mathematics and Computation Branch
Chalk River Laboratories
Chalk River, Ontario, Canada, K0J 1J0
1992 March

AECL-10583

TABLE OF CONTENTS

1. INTRODUCTION

Relativistic large-amplitude electron plasma waves are encountered in controlled thermonuclear fusion research, advanced particle accelerator research and space plasma research. These waves are important in hot electron preheat in laser fusion targets, current drive in tokamaks, laser acceleration of particles and final focusing of particle beams in high-energy particle accelerators. In the area of particle acceleration, there are at least three concepts for plasma-based collective accelerators, all of which involve plasma waves with phase velocities almost equal to the velocity of light, and plasma wave amplitudes that are a significant fraction ($\geq$ 10%) of the cold-plasma wavebreaking limit. In the laser plasma beatwave accelerator (LPBWA) concept proposed by Tajima and Dawson,[1] the plasma waves are generated by the nonlinear coupling of two intense laser beams of slightly different frequencies propagating through a low-density plasma. If the difference frequency of the lasers is chosen to match the plasma frequency, the ponderomotive force of the beatwave can resonantly build up the relativistic plasma wave. In the plasma wakefield accelerator (PWFA) concept, the plasma waves are excited by a short, intense electron bunch propagating through a high-density plasma.[2] The space charge force of the electron bunch displaces the plasma electrons and generates a wake of plasma oscillations with a phase velocity that is equal to the driving electron bunch velocity, which is very close to the velocity of light. An alternative to using an electron bunch is to inject an extremely short but intense laser pulse into a low-density plasma, as is the case in the laser wakefield accelerator (LWFA) concept.[3] The ponderomotive force of the laser pulse envelope initially expels the plasma electrons both radially and axially, resulting in plasma oscillations as the returning electrons overshoot their initial positions.

The acceleration of particles in the three concepts is identical. A trailing relativistic electron bunch injected into the potential well of the plasma wave at the appropriate phase remains synchronized to the wave and accelerated for a significant period of time.

In this report, we discuss the results of a study of electron acceleration by relativistic large-amplitude electron plasma waves. Although particular reference is made to the laser

plasma beatwave concept, the study is equally relevant to the acceleration of particles in the plasma wakefield accelerator and the laser wakefield accelerator.

In the laser plasma beatwave concept two laser pulses of frequency ω_0 and ω_1 are injected into a plasma with a plasma frequency ω_p. If ω_0 and ω_1 are both greater than ω_p, the laser pulses propagate through the plasma without attenuation (i.e., the plasma is underdense to the incoming electromagnetic radiation). In the presence of the transverse electric field of the laser pulses, each free electron in the plasma oscillates in a direction perpendicular to the direction of propagation of the laser beams. The wave magnetic field displaces the plasma electrons along the direction of light propagation, depending on the field strength and the instantaneous electron velocity. If the intensity of the laser light is constant along the direction of propagation, the electric and magnetic forces experienced by the plasma electrons during one half cycle of oscillation is equal and opposite to the next half cycle, and the electrons return to their starting position at the end of each oscillation. If the intensity of the laser light varies along the direction of propagation (as in the case of the beating of two laser beams of slightly different frequencies), the plasma electrons experience varying electric and magnetic fields during each half cycle of oscillation. The net effect does not cancel exactly during a period of oscillation, and plasma electrons pile up along the direction of light propagation. This phenomenon is known as the ponderomotive effect. It results from the nonlinearity of spatially-varying electromagnetic fields. As a result of the ponderomotive effect, a space-charge wave due to the displaced plasma electrons builds up behind a laser pulse. If the frequency of the beating light envelope, $\Delta\omega = \omega_0 - \omega_1$, is resonantly matched to the plasma frequency, ω_p (natural vibration frequency in a plasma), the ponderomotive force on the plasma electrons maintains a resonance with the plasma frequency, and the amplitude of the space-charge wave grows significantly, often reaching a significant fraction ($\sim$ 30%) of the background electron density. Thus very large electric field gradients are created.

In a laser beam of constant amplitude, each oscillating plasma electron experiences increasing displacement from its equilibrium position and increasing peak velocity. Eventually, the relativistic mass increase of a plasma electron due to these peak velocities shifts the plasma

frequency out of resonance with the beat frequency. The amplitude of the space-charge wave begins to decrease, thereby reducing the peak velocities. On a longer timescale, the amplitude varies harmonically, exchanging energy back and forth with the beating laser beams. If the incoming laser beam intensity is not constant, but has a finite risetime and pulse duration, the initial buildup of the space-charge wave will take longer, then continue to change harmonically, and finally decay away after the laser pulse has passed.

It has been proposed[1] that the potential well associated with the large-amplitude electron plasma waves can be used to accelerate particles injected from an external source to ultra-relativistic energies. The maximum acceleration that can be obtained from this process depends on many different factors. This report presents a study of how these various factors impact on the acceleration mechanism. For instance, the time of injection of the particles during the buildup time of the space-charge wave, the injection phase of the particles relative to the potential troughs, the injection energy of the particles and the acceleration length of the interaction region are all relevant issues that determine the maximum energy gain of the particles. Clearly, some of these factors will be tempered by experimental issues. In present-day experiments, injection phases are not easily controlled, and energy spread in the output spectrum will occur. Radial forces from the space-charge wave will influence the maximum acceleration as well as the spot size of the accelerated beam. Ideally, the experimentally attainable length of the interaction region should be matched to the acceleration length.

The issues raised in the foregoing discussion are studied in a series of model calculations, which help to demonstrate the basic physics and provide greater insight into the various mechanisms underlying this concept. The range of parameters used in these studies to demonstrate the physical principles have been selected from those typical of present-day experiments.[4,5]

2. THEORY AND SIMULATIONS

(i) Plasma Wave Generation

In the laser plasma beatwave acceleration concept, the plasma waves are generated by the non-linear coupling of two co-propagating laser beams in a low-density plasma. The periodic force that acts on the plasma electrons (ponderomotive force) and causes them to bunch is directed along the propagation direction of the electromagnetic waves. It originates in a non-zero **v** x **B** force due to the electromagnetic waves (Fig. 1). The ponderomotive force is given by[6]

$$\boldsymbol{F}_{NL} = - \frac{\omega_{pe}^{2}}{\omega_0 \omega_1} \varepsilon_0 \nabla \frac{< | \boldsymbol{E}_0 + \boldsymbol{E}_1 |^2 >}{2} \qquad (1)$$

where $\omega_{pe} = (n_e e^2/\epsilon_0 m_e)^{1/2}$ is the electron plasma frequency, n_e is the plasma electron density, ω_0 and ω_1 are the laser frequencies, $\mathbf{E}_0$ and $\mathbf{E}_1$ are the electric fields of the two laser beams and ϵ_0 is the permittivity of free space.

Consider two plane electromagnetic waves with frequencies ω_0 and ω_1 polarized in the x-direction and propagating in the z-direction with equal electric field amplitudes. The combined electric field is

$$\begin{aligned} \boldsymbol{E} &= \boldsymbol{E}_0 + \boldsymbol{E}_1 \\ &= E_0 [\cos(k_0 z - \omega_0 t) + \cos(k_1 z - \omega_1 t)] \boldsymbol{x} \\ &= 2E_0 \cos[(k_0+k_1)\frac{z}{2} - (\omega_0+\omega_1)\frac{t}{2}] \cos[(k_0-k_1)\frac{z}{2} - (\omega_0-\omega_1)\frac{t}{2}] \boldsymbol{x} \end{aligned} \qquad (2)$$

The high-frequency component of the beatwave is at the average frequency $(\omega_0 + \omega_1)/2$, whereas the beatwave envelope is at the frequency $(\omega_0 - \omega_1)/2$.

Using Eqn. (1) and averaging over the short time scale $\omega^{-1} = 2/(\omega_0 + \omega_1)$, the force on each m^{-3} of fluid (ponderomotive force $\mathbf{F}_{NL}$) is obtained from

$$< \boldsymbol{E}^2 >_{\frac{1}{\omega}} = 2E_0^2 \cos^2[(k_0 - k_1)\frac{z}{2} - (\omega_0 - \omega_1)\frac{t}{2}] \qquad (3)$$

as

$$\boldsymbol{F}_{NL} = - \frac{\varepsilon_0 \omega_{pe}^2}{2\ \omega_0 \omega_1} E_0^2\ \Delta k \sin\ (z\Delta k - t\Delta\omega)\boldsymbol{Z} \qquad (4)$$

where $\Delta k = k_0 - k_1$ and $\Delta\omega = \omega_0 - \omega_1$.

We can estimate the maximum possible amplitude of the plasma wave by considering the maximum possible bunched electron density or density fluctuation δn_e. For a background plasma electron density of n_e, the maximum possible density fluctuation $\delta n_e = n_e$ (Fig. 1).

From Poisson's equation

$$\nabla\cdot\boldsymbol{E} = \frac{\rho}{\varepsilon_0} = - \frac{1}{\varepsilon_0} e\delta n_e = - \frac{1}{\varepsilon_0} e n_e, \qquad \delta n_e \approx n_e \qquad (5)$$

$$\nabla^2\phi \approx \frac{1}{\varepsilon_0} e n_e \qquad (6)$$

and

$$|e\phi| \approx \frac{n_e e^2}{\varepsilon_0 m_e}\frac{m_e}{k^2} = \frac{\omega_{pe}^2}{c^2 k^2} m_e c^2 \qquad (7)$$

The maximum electric field

$$|\boldsymbol{E}_{max}| = |k\phi_{max}| = \frac{\omega_{pe} m_e c^2}{ce} = 0.096\sqrt{n_e} \quad V/m \qquad (8)$$

where n_e is the plasma electron density in m^{-3}.

For the general case the amplitude of the density fluctuation $\varepsilon = \delta n_e/n_e$ can be obtained from the Maxwell and fluid equations within the slowly varying envelope approximation[7-10]

$$\left(\frac{1}{\omega_{pe}}\frac{d}{dt} - i\frac{3}{16}|\varepsilon|^2 + i\frac{\Delta\omega}{\omega_{pe}} - \frac{\nu_e}{2\omega_{pe}}\right)\varepsilon = \frac{1}{4}\alpha_0\alpha_1 \qquad (9)$$

where $\Delta\omega = \omega_{pe} - (\omega_0 - \omega_1)$ is the frequency detuning from exact resonance, ν_e is the electron-ion collision frequency and $\alpha_1 = v_{o1}/c = eE_1/m_e\omega_1 c$ is the normalized oscillatory velocity of an electron in the laser field E_1. The driver term on the right-hand side of Eqn. (9) is defined in terms of the laser field strengths (E_0 and E_1) of the two laser beams. The second term on the left-hand side, which gives a nonlinear frequency shift as the plasma wave amplitude increases, is due to the relativistic mass increase of the oscillating electrons as $m_e \rightarrow \gamma m_e$ and $\omega_{pe}^2 \rightarrow \omega_{pe0}^2/\gamma$, where ω_{pe0} is the plasma frequency with the rest mass, and γ is the relativistic Lorentz factor defined by the mean electron velocity in the wave. The third term describes a linear detuning of the plasma frequency ω_{pe} from the exact resonance with the beat frequency $(\omega_0 - \omega_1)$. The fourth term is the linear damping term due to electron-ion collisions.

Equation (9) shows that the plasma wave amplitude initially grows linearly with time according to the relation

$$\frac{1}{\omega_{pe}}\frac{d\varepsilon}{dt} = \frac{1}{4}\alpha_0(t)\alpha_1(t) \qquad (10)$$

In the absence of other effects, relativistic detuning limits the amplitude of the plasma wave. As the plasma wave grows, the plasma electrons increase in mass and the plasma frequency ω_{pe} no longer matches the driver frequency $(\omega_0 - \omega_1)$; this dephasing causes the amplitude growth to slow, stop and then reverse.[11] The saturated amplitude is given by

$$\varepsilon_s = [\frac{16}{3}\alpha_0(t)\,\alpha_1(t)]^{\frac{1}{3}} \qquad (11)$$

and the time to saturation is determined from

$$\frac{\omega_{pe}}{4}\int_0^{\tau_s}[\alpha_0(\acute{t})\,\alpha_1(\acute{t})]\,d\acute{t} = [\frac{16}{3}\alpha_0(t)\,\alpha_1(t)]^{\frac{1}{3}} \qquad (12)$$

Assuming a linear risetime τ for the laser intensity, $I(t) = It/\tau$ and $\alpha(t) = \alpha\,(t/\tau)^{1/2}$, the time to saturation is given by

$$\omega_{pe}\tau_s = 4.87\,[\frac{\tau\omega_{pe}}{\alpha_0\alpha_1}]^{\frac{2}{5}} \qquad (13)$$

The saturated electric field amplitude is then given by

$$E_s = 0.096\,\sqrt{n_e}\,\varepsilon_s \qquad V/m \qquad (14)$$

For maximum plasma wave amplitude, the time to saturation, Eqn. (13), should be matched to the laser pulse duration. There is also an advantage to choosing a plasma density so that the exact frequency match between the driver and the plasma frequency occurs not at the beginning of the laser pulse, but later on, during the growth when the laser intensity is greater.[11] This detuning can increase the saturated amplitude by as much as 60%. It has been suggested that the plasma density could be continuously adjusted to maintain exact resonance at all times during the laser pulse, and a number of approaches have been suggested to achieve this in practice.[12]

For resonant excitation of plasma waves (frequency ω_p and wavenumber k_p) with two copropagating laser beams of frequency ω_0 and ω_1 and wavenumbers k_0 and k_1, respectively, the following wavematching relations must be satisfied

$$\omega_p = \omega_0 - \omega_1 = \Delta\omega \qquad \boldsymbol{k}_p = \boldsymbol{k}_0 - \boldsymbol{k}_1 = \Delta\boldsymbol{k} \qquad (15)$$

The phase velocity of the plasma wave v_p is given by

$$v_p = \frac{\omega_p}{k_p} = \frac{\omega_0 - \omega_1}{k_0 - k_1} = \frac{\Delta\omega}{\Delta k} = v_g^{EM} \qquad (16)$$

where the group velocity of the electromagnetic waves v_g^{EM} is obtained from the dispersion relation for an electromagnetic wave in a plasma

$$\omega^2 = \omega_{pe}^2 + k^2c^2 \qquad (17)$$

The group velocity is

$$v_g^{EM} = \frac{d\omega}{dk} = \frac{kc^2}{\omega} = c\left(1 - \frac{\omega_{pe}^2}{\omega^2}\right)^{1/2} \qquad (18)$$

The phase velocity is then given by

$$v_p = c\left(1 - \frac{\omega_{pe}^2}{\omega^2}\right)^{1/2} \qquad (19)$$

and the Lorentz factor γ_p is defined as

$$\gamma_p = \left(1 - \frac{v_p^2}{c^2}\right)^{-1/2} = \left(\frac{\omega}{\omega_{pe}}\right) = \left(\frac{n_c}{n_e}\right)^{1/2} \qquad (20)$$

where n_c is the critical density for the laser beam (where the laser frequency equals the plasma frequency), which for a CO_2 laser is $n_c = 10^{25}$ m^{-3}.

An important feature of laser accelerators is the synchronism that exists between the group velocity v_g of the laser pulse and the phase velocity of the plasma waves, as shown in Eqns. (18) and (19). It follows that the trapped particles being accelerated are also in synchronism with the laser pulse, and particles are accelerated by the electrostatic wave until they outrun the wave. The maximum energy gain

$$\Delta W \approx 4\ \varepsilon_s\ \gamma_p^2\ m_e\ c^2 \qquad (21)$$

The dephasing distance is

$$L_p = \frac{1}{2} \lambda_p \gamma_p^2 \qquad (22)$$

Equation (22) is nothing more than a statement that when a particle accelerates, it can move from the top to the bottom of the potential well of the plasma wave. In other words, it can travel, at most, half a plasma wavelength in the (moving) wave frame.

Experimental parameters typical of present-day experiments[4,5] calculated from Eqns. (9) through (22) are given in Table 1 for plasma densities of 10^{22} and 10^{23} m^{-3}. Since the phase velocity of the plasma wave is somewhat lower at the higher electron densities (Eqn. 20), the injection energy of the particles for trapping is also lower.

(ii) <u>One-dimensional Model</u>

A simple one-dimensional model gives a great deal of insight into the basic physical mechanism for particle acceleration in relativistic electron plasma waves. Consider the relativistic motion of an electron in a large amplitude plasma wave, as shown in Fig. 2. If an incoming electron is moving too slowly with respect to the plasma wave, then the plasma wave outruns the particle before it can experience any acceleration. If, on the other hand, the incoming electron is moving too fast with respect to the plasma wave, then it outruns the wave, and once again experiences no acceleration. Hence there is a minimum and maximum injection energy of the electron for which the electron is trapped by the plasma wave. These limits are most easily determined by considering the motion of the particle in the wave frame (Fig. 2). In the laboratory frame, the energy and velocity of the electron are given by $\gamma = (1 - \beta^2)^{-1/2}$ and $\beta = v/c$. The Lorentz factor, the phase velocity, the electric field amplitude, the electric potential and the wavenumber for the plasma wave in the laboratory frame are given by γ_p, β_p, E, ϕ and k_p, respectively. The energy and velocity of the electron in the wave frame are given by γ^{wave} and β^{wave}. The corresponding values in the wave frame for the electric field amplitude, the electric potential and the plasma wavenumber are given by E^{wave}, ϕ^{wave} and k_p^{wave}.

The electron energy and velocity in the two frames are related by the Lorentz transformations

$$\gamma^{wave} = \gamma\gamma_p \ (1 - \beta\beta_p) \tag{23}$$

and

$$\gamma = \gamma^{wave}\gamma_p \ (1 + \beta^{wave}\beta_p) \tag{24}$$

The wavenumber, k^{wave}, of the plasma wave in the wave frame is obtained by the Lorentz transformations of the momentum four-vectors for the plasmon

$$\begin{pmatrix} \gamma & i\beta\gamma \\ -i\beta\gamma & \gamma \end{pmatrix} \begin{pmatrix} k_p \\ i\omega_p/c \end{pmatrix} = \begin{pmatrix} k_p/\gamma \\ 0 \end{pmatrix} \tag{25}$$

where the right-hand side refers to the wave frame quantities.

Hence

$$k_p^{wave} = \frac{k_p}{\gamma} \tag{26}$$

The equation of motion of the electron must transform similarly under a Lorentz transformation. However, despite the fact that both the mass and acceleration are different in the two frames, the component of force along the direction of motion remains the same in special relativity where one frame is at rest. Hence $\mathbf{E} = \mathbf{E}^{wave}$.

The wave potential in the laboratory frame is given by

$$\boldsymbol{E} = \boldsymbol{E}^{wave} = -\nabla\phi = -\boldsymbol{k}_p\phi \tag{27}$$

Using the invariance of the electric field under Lorentz transformation ($\mathbf{E} = \mathbf{E}^{wave}$), and Eqns. (26) and (27), the wave potential in the wave frame is

$$e\phi^{wave} = -\frac{e\,E^{wave}}{k_p^{wave}} = -\frac{e\,E}{k_p^{wave}} = \frac{k_p}{k_p^{wave}}\, e\,\phi = \gamma_p e\phi = \gamma_p mc^2 \tag{28}$$

In the wave frame, the picture is now quite simple. The plasma wave is a standing space charge wave of wavenumber k_p/γ_p and electric field amplitude $\mathbf{E} = \mathbf{E}^{wave}$. The electric potential of the plasma wave $\phi^{wave} = \gamma_p\phi$ (Fig. 2). In order to trap the incoming electron, the kinetic energy of the electron in the wave frame must be less than the potential well of the standing wave

$$(\gamma^{wave} - 1)\, mc^2 \leq e\phi^{wave} \tag{29}$$

The above condition is written in laboratory frame quantities using Eqns. (24) and (26) for the transformations of the energy and the wavenumber, respectively, and the invariance of the electric field. Minimum laboratory frame energy for an electron trapped in a plasma wave is then obtained as

$$\gamma_{min} = \gamma_p\left(1 + \frac{\Gamma e\phi^{wave}}{mc^2}\right)\left[1 - \beta_p\left(1 - \frac{1}{\left(1 + \frac{\Gamma e\phi^{wave}}{mc^2}\right)^2}\right)^{\frac{1}{2}}\right] \tag{30}$$

where $\Gamma = (1 + \cos\phi_0)$ and ϕ_0 is the phase at which the particle is injected into the plasma wave.

Maximum laboratory frame energy for an electron is obtained when it reverses its acceleration in the wave frame. Using the transformations given above, the maximum laboratory frame energy is given by

$$\gamma_{max} = \gamma_p\left(1 + \frac{\Gamma e\phi^{wave}}{mc^2}\right)\left[1 + \beta_p\left(1 - \frac{1}{\left(1 + \frac{\Gamma e\phi^{wave}}{mc^2}\right)^2}\right)^{\frac{1}{2}}\right] \tag{31}$$

The relativistic equation of motion of an electron in an electric field in one dimension is

$$\frac{d}{dt}(\gamma m_e \boldsymbol{v}) = -e\boldsymbol{E}\sin(k_p z - \omega_p t + \phi_0) \tag{32}$$

where the injection phase ϕ_0 is relative to the plasma wave.

If $\xi = k_p z - \omega_p t$, then Equation (32) can be reduced to the differential system

$$\frac{d}{dt}(\gamma\beta) = -\left(\frac{eE}{m_e c}\right)\sin(\xi + \phi_0)$$
$$\frac{d\xi}{dt} = ck_p\beta - \omega_p \qquad (33)$$

The first-order ordinary differential equation in $d\gamma/d\xi$ from Equation (33) can be solved analytically in terms of the variables (γ,ξ) with the solution

$$\gamma - \beta_p(\gamma^2-1)^{\frac{1}{2}} - A\cos(\xi+\phi_0) = \gamma_0 - \beta_p(\gamma_0^2-1)^{\frac{1}{2}} - A\cos(\xi_0+\phi_0) \qquad (34)$$

where $A = (eE)/(mc^2k_p)$, $\beta_p = \omega_p/(k_p c)$, and the initial values are (γ_0,ξ_0).

To help visualise the motion of the electron more clearly, we refer to the electric field of the plasma wave and the electric potential in the wave frame, together with the forces on the electron shown in Fig. 3. The Lorentz factor for the plasma wave $\gamma_p = 32$. Consider a particle injected into the wave with an initial energy of 5 MeV ($\gamma = 10$) at zero phase, which corresponds to a zero in the electric field and a potential minimum, in the wave frame. In the lab frame the particle is moving in the same direction as the wave, but slower. In the wave frame the particle is initially moving in the negative z-direction. If the particle is to be trapped by the plasma wave, it must, at least, come to rest at the top of the potential well, i.e., its kinetic energy in the wave frame must not exceed the depth of the potential well (as stated in Eqn. (29)). The particle then moves down the potential well (i.e., in the positive z-direction), and acquires its maximum energy when it reaches the bottom of the potential well (as stated in Eqns. (21) and (31), and the discussions that follow). The reason relativistic particles gain energy very rapidly is as follows. Since $\gamma = (1 - \beta^2)^{-1/2}$ and $\beta = v/c$ then

$$\frac{d\gamma}{\gamma} = (\gamma^2-1)\frac{d\beta}{\beta} \qquad (35)$$

For small fractional changes in the particle velocity (i.e., $d\beta/\beta$) large fractional changes in the particle energy ($d\gamma/\gamma$) are obtained because of the non-linear relationship (in γ^2) between the two

quantities. Physically, this means that when a relativistic particle is accelerated, it increases in mass rather than velocity.

Figure 4 (a) shows the particle orbits in phase space (γ,ξ) for particles injected with different initial energies into a plasma wave with a wave amplitude $\epsilon = 0.24$ (i.e., $E_0 = 2.4$ GeV/m) and a background electron plasma density of 10^{22} m^{-3}. In phase space the picture is as follows. The particle is injected at zero phase at point A in Fig. 4 (a). Initially, the particle slips in phase (gaining only a small amount of energy) until it reaches the point B. It then gains energy very rapidly until it reaches the maximum energy at point C. From point C to A, the particle advances in phase, losing energy until it arrives at point A again and the cycle repeats itself. Points A,B and C are also shown in Fig. (3), which also shows the forces acting on the particle at different points on the particle orbits in phase space.

The location of point B is determined by noting that in phase space, B corresponds to the location of the vertical tangent to the particle orbit. Then from Eqn. (34)

$$\frac{d\gamma}{d\xi} = \frac{-A\,(1-\frac{1}{\gamma^2})^{\frac{1}{2}}\sin\xi}{(1-\frac{1}{\gamma^2})^{\frac{1}{2}} - \beta_p} \qquad (36)$$

The vertical tangent is obtained when $d\xi/d\gamma = 0$, i.e., $\gamma = \gamma_p$, and so

$$(\gamma_p - \gamma_0) - \beta_p\,(\gamma_p^2 - 1)^{\frac{1}{2}} - \beta_p\,(\gamma_0^2 - 1)^{\frac{1}{2}} + A\cos\xi_0 = A\cos\xi_T \qquad (37)$$

from which the phase angle ξ_T corresponding to the vertical tangent can be obtained. B is the turning point where the particle initially moving along the negative z-direction in Fig. 3 is stopped, turned around and trapped by the wave. The trapped particle moving down the potential well gains energy very rapidly until it reaches the bottom of the potential well and then starts to climb up the potential well on the other side, thereby losing energy. The centre of the

particle orbit in phase space (O) corresponds to $\gamma = \gamma_r$, where the particle neither gains nor loses energy but remains in a constant phase of zero. Orbit P corresponds to a particle whose initial energy γ is less than γ_{min} and Q corresponds to a particle with initial energy greater than γ_{max}. These orbits describe the untrapped particles. The thick lines on these trajectories describe the particle motion for 45 plasma wave periods ($2\pi\omega_{pe}^{-1}$) or 1.5 cm acceleration length, which is typical of our experiments.

Figure 4 (b) shows a plot of the maximum output energy of the particles as a function of the lab distance z for zero injection phase and a set of initial injection energies. The lab frame distance z is normalized by the plasma wavenumber $k_p = 2\pi/\lambda_p$, where λ_p is the wavelength of the plasma wave. This figure shows that the maximum output energy of the particles is periodic, with the lab distance z, as expected from Fig. 4 (a). For maximum output energy the length of the accelerating region should be tailored to correspond to one of the maxima in the output energy.

Figure 4 (c) shows the output energy of particles with an initial energy of 10 MeV, as a function of the lab frame distance z for a number of different values of the injection phase ϕ_0. The maximum energy is obtained for particles that are initially injected with a phase of greater than $\pi/2$. In the laser plasma beatwave experiments, since there is no selection of the injection phases of the individual particles, a spectrum of electron energies may be expected. Figure 4 (d) shows a plot of the output energy of particles injected uniformly in all phases between 0 and π for an initial injection energy of 10 MeV and a plasma length $z = 1.5$ cm ($k_p z = 295$). Particle trapping and significant energy gain is obtained for particles injected within approximately $\pm \pi/2$, centred on $\pi/2$. Figure 4 (e) shows a plot of the final phase of the particles as a function of the initial phase, for an initial injection energy of 10 MeV.

Figure 4 (f) shows a typical output energy spectrum for 10 MeV particles injected with injection phases uniformly distributed between 0 and $\pi/2$. For this particular case, the maximum energy gain is approximately 36 MeV, which agrees well with Eqn. (21).

In actual experiments, the electric field amplitude of the plasma wave will have an axial variation, as a result of the focusing geometry of the laser beam. To simulate this effect, the calculations discussed in Figs. 4 (a) - 4 (f) were repeated using modulated accelerating field amplitudes given by

$$E = E_0 f(z)$$

$$f(z) = \frac{1}{(1 + \frac{z^2}{z_r^2})^{\frac{1}{2}}} \qquad (38)$$

where $z_r^2 = (\pi w_0^2/\lambda)^2$ is the Rayleigh range, z is the axial distance measured from the laser beam waist, $z = 0$ corresponds to the laser beam waist with spot size w_0, and λ is the laser wavelength.

Figure 5 (a) shows the spatial profile of the constant amplitude (plane wave) electric field with $f(z) = 1$ used in the calculations discussed so far. Figure 5 (b) shows the amplitude-modulated field, which results from the focusing geometry of the laser beam.

Figure 6 (a) shows the output energy as a function of the axial lab frame distance z for an injection phase of zero and a set of injection energies. Comparing Figure 6 (a) with the corresponding calculations for a plane wave with $f(z) = 1$, in Fig. 4 (b), the maximum output energy is observed to be lower for the case of an axially varying field amplitude, compared to the plane wave case, where the amplitude is independent of the axial distance z. Furthermore, the modulated field amplitude case does not show the periodic behaviour in the output energy that was observed in the plane wave case. Figure 6 (b) shows the output energy as a function of the axial lab distance for 10 MeV particles injected with a number of different phases. Again the periodic variation of the output energy is less pronounced than in the previous case. Figure 6 (c) shows the corresponding output energy spectrum, which shows not only a lower

maximum energy, but also a different spectral distribution of energies compared to Fig. 4 (f). Another important feature of the acceleration process with an axially varying field is the increase in the threshold (or minimum) energy for particle trapping compared to the plane wave case, which is given by Eqn. (30). A particle with a minimum energy that is trapped in a plane wave will not necessarily be trapped in a wave that has an axial amplitude modulation. In order to gain some physical insight into this behaviour of the particles as observed in the computer simulations, we use a simple mathematical model, which shows qualitatively the features predicted by the simulations. Consider a function for the plasma wave amplitude with a linear leading edge of length Z, i.e.,

$$E(z) = E_0 f(z) \sin (k_p z - \omega_p t + \phi_0) \qquad (39)$$

where $f(z) = z/Z$ gives a linear leading edge shown in Fig. 7. The linear leading edge is chosen to simplify the integration on the right-hand side of Eqn. (39). The energy change of a particle of charge q starting at $z = t = 0$ with a phase ϕ_0 and ending at Z is given by

$$W = q \int_0^Z dz\, E \frac{z}{Z} \sin (k_p z - \omega_p \frac{z}{v} + \phi_0) \qquad (40)$$

By substituting ϕ as the outgoing phase, we obtain

$$y = \phi - k_p \left(1 - \frac{v}{c}\right) z + \phi_0 \qquad (41)$$

and

$$W = q \int_{\phi_0}^{\phi} \frac{E}{k_p \left(1 - \frac{v}{c}\right)} \frac{v}{c} \left(y - \phi_0\right) \sin y \, dy \qquad (42)$$

With the assumption that an average $\langle v \rangle = v$ can be defined, then

$$W = \frac{qE_0}{k_p\left(1 - \frac{v_p}{v}\right)} - \left[-\cos\phi + \frac{(\sin\phi - \sin\phi_0)}{Zk_p\left(1 - \frac{v_p}{v}\right)}\right] \qquad (43)$$

Equation (43) can now be used to explain qualitatively what is observed in the simulation. If the leading edge is gradual, the second term in Eqn. (43) is small, because Z is large and $Zk_p(v_p/v - 1) >> 1$. Thus we have a modulation of the electron energy given by the first term as a sinusoidal function of ϕ, and W is most negative when ϕ is close to π. This is what is observed in the simulations. In fact, the amplitudes of modulation in the simulations agree well with the value $qE_0/k_p(1 - v_p/v)$, indicating the validity of the use of a fixed v. The v used was the injection electron speed. For a steep leading edge, $Zk_p(v_p/v - 1) >> 1$ is not satisfied. The second term in Eqn. (43) is positive at $\phi = \pi$ and non-negligible compared to the first term. Therefore, the modulation is reduced.

(iii) Two-dimensional Model

The finite width of the laser beams (radius r_0) results in a transverse variation of the space-charge wave, which gives rise to radial focusing and defocusing fields. These radial fields can set up betatron oscillations for the injected particle beam. If the longitudinal field has a radial variation given by

$$E_z(r) = E_{z0}\left(1 - \frac{r^2}{r_0^2}\right) \qquad (44)$$

then from Maxwell's equations it can be shown that the radial field has the form[13]

$$|E_r| = |E_{z0}|\,\frac{2r}{k_p r_0^2} \qquad (45)$$

The radial field E_r is $\pi/2$ out of phase with the longitudinal field E_z, so that it is focusing or defocusing according to the phase, and one half of the accelerating cycle is radially focusing and one half is radially defocusing, as shown in Fig. 8. The expressions for the longitudinal and

radial fields generated by the beatwave can be derived in the linear fluid approximation for an unmagnetized, cold plasma of classical electrons and immobile ions[14]

$$E_z(r,z,t) = -\left[\frac{m_e c\omega_p}{e}\right] \alpha\, e^{-\frac{2r^2}{R^2}} \times \left[\omega_p t\cos(k_p z-\omega_p t) + \cos(k_p z)\sin(\omega_p t)\right] \tag{46}$$

$$E_r(r,z,t) = -4\left[\frac{m_e c\omega_p}{e}\right] \alpha\, \frac{r}{k_p R^2} e^{-\frac{2r^2}{R^2}} \times \{\omega_p t\sin(k_p z-\omega_p t) - 2[1-\cos(\omega_p t)] - \sin(k_p z)\sin(\omega_p t)\} \tag{47}$$

where the two laser pumps are assumed to have the form given in Eqn. (2). Equations (46) and (47) predict the longitudinal and radial field profiles for the plasma waves in the linear regime up to saturation. A plot of the longitudinal field profiles given by Eqns (46) and (47) is shown in Fig. 9. Ideally, particles should be injected in the accelerating and focusing phase (Fig. 8), in which case the accelerated beam is likely to be tightly focused. In the defocusing phase, on the other hand, the particles are likely to be scattered.

A modification to Eqns. (46) and (47) has been introduced to take into account the axial variation in the intensity of the focused laser beams. The modified forms of Eqns. (46) and (47) used in the present calculations are given by

$$E_z(r,z,t) = -\left[\frac{m_e c\omega_p}{e}\right] \alpha e^{-\frac{2r^2}{R^2}} f(z) \times \{\frac{4z}{k_p\sigma^2}[2(1-\cos(\omega_p t)) + \sin(k_p z)\sin(\omega_p t) - \omega_p t\sin(k_p z-\omega_p t)] + [\sin(k_p z)\cos(\omega_p t) + \omega_p t\cos(k_p z-\omega_p t)]\} \tag{48}$$

$$E_r(r,z,t) = -4\left[\frac{m_e c\omega_p}{e}\right]\alpha\frac{r}{k_p R^2}e^{-\frac{2r^2}{R^2}}f(z)$$

$$\times\{\omega_p t\sin(k_p z-\omega_p t)-2[1-\cos(\omega_p t)]$$

$$-\sin(k_p z)\sin(\omega_p t)\} \qquad (49)$$

where $f(z) = \exp(-2z^2/\sigma^2)$, and σ is the beam waist, and z is centred on the beam waist. In our calculations, where the electrons are injected from the near field, the origin of the z-axis has to be shifted.

Equations (48) and (49) are based on a linearized theory that is valid for initial plasma wave growth up to saturation. For injecting particles close to the peak of the accelerating field (i.e., saturation fields), Eqns. (48) and (49) must be further modified to take into account the non-linear behaviour of the plasma waves, since otherwise the fields will continue to grow beyond the saturation limit during the time the particle takes to traverse the accelerating region. To implement this, we use a one-dimensional, non-linear, fully relativistic model of the plasma wave and numerically integrate the differential equations for the wave amplitude and the phase to obtain the wave amplitude as a function of time.[11] Figure 10 shows that the wave amplitude initially grows linearly with time until the relativistic mass increase shifts the plasma frequency out of resonance with the laser driver. This results in a decrease in the wave amplitude. Physically, the phase difference between the laser driver and the plasma wave (Fig. 11) changes sign, which results in energy flow from the plasma wave to the laser field. In fact, there is a periodic exchange of energy between the laser driver and the plasma wave, as shown in Fig. 11.

The particles are now injected during the plasma wave buildup before the peak fields are obtained, accelerate through the region as the wave amplitude reaches the maximum value, and then decrease as the plasma wave gives its energy to the laser fields. This approach is consistent with a model in which the particles are injected with the average value of the plasma wave amplitude, and the amplitude is maintained at a constant value. Figure 12 shows an energy

spectrum of accelerated particles in one dimension for a fixed field amplitude (a) and a linearly-rising field amplitude calculated using the relativistic, non-linear model (b). The excellent comparison between the two calculations for on-axis particles shows a good degree of consistency between the two models.

Figure 13 shows the wave amplitude as a function of time for a finite duration laser pulse, with a risetime of 250 ps and a full-width-half maximum duration of 500 ps. The wave amplitude builds up to a maximum, undergoes a number of oscillations during the laser pulse as the laser driver and the plasma waves exchange energy, and finally decays as the laser pulse turns off.

Figure 14 shows the motion of particles injected off-axis at a normalized radius $k_p r = 1$, for a number of different injection phases between 0 and π. For injection phases greater than $\pi/2$, the particles rapidly move away from the axis as they propagate through the beatwave region, as expected for the radially defocusing fields shown in Fig. 8. For injection phases between 0 and $\pi/2$, where the radial field is focusing, the particles execute the normal betatron oscillations about the axis of the system. The maximum longitudinal axis displayed in Fig. 14 corresponds to the maximum dimension of the accelerating region in a typical experiment (approximately 1.5 cm).

In Fig. 14, all the particles have been injected parallel to the z-axis. The present calculations are based on a cylindrically symmetric model and negative values of the variable r have been used to indicate where the particles cross the propagation axis.

Figure 15 shows the motion of particles injected at a phase angle of $\pi/4$, for a number of different off-axis positions. The particles all invariably diverge away from the propagation axis.

Figure 16 shows the motion of particles injected at a number of different off-axis locations for an initial phase angle of $\pi/2$. The particles in this case are in the radially defocusing phase and continue to diverge as they propagate through the accelerating region.

Figure 17 shows the motion of particles that are injected at the optimum phase for maximum output energy (ϕ_0 = 90° to 110°) for a number of different off-axis positions. For these conditions the particles are focused as they converge towards the propagation axis. For conditions similar to this but at an injection phase of 135° (Fig. 18), the particles execute betatron oscillations as they propagate along the axis.

Figure 19 shows a plot of the optimum injection phase for maximum output energy as a function of the radial position of the particle for off-axis injection. From this plot the optimum injection phase for a range of off-axis positions appears to be approximately 95°. Since the radial field is maximum off-axis, the maximum output energy also decreases with increasing off-axis distance (Fig. 20).

(iv) Two-Dimensional Model with Beam Emittance

It is customary to represent a particle beam travelling along the axial z-direction as a 6-dimensional ellipsoid in phase space. In the parametric representation, the ellipsoid is characterized with the six parameters (x_m,θ_m,y_m,φ_m,L,δ), where x_m is the lateral displacement perpendicular to the z-axis, θ_m = dx/dz is the divergence in the x-z plane, y_m is the lateral displacement perpendicular to both the x and the z axis, φ_m = dy/dz is the divergence in the y-z plane, L is the longitudinal beam extent and δ is the momentum spread.

If the ellipsoid is projected into a two-dimensional subspace (x_m,θ_m), the result is an ellipse in this phase space (x_m,θ_m). For modeling the radial motion of the particles, the longitudinal projection of the ellipsoid can be neglected, provided there is no coupling between the radial and longitudinal motions. Furthermore, if azimuthal symmetry is assumed, the ellipses in the (x_m,θ_m) and (y_m,φ_m) subspaces are identical, and it suffices to consider the behaviour of the particles in the (x_m,θ_m) subspace only.

In our model we consider the distribution of particles in the (r_m,θ_m) subspace. In order to illustrate some of the points discussed above, we have selected two cases with different

distributions for the injected particles. In the first case, we assume a beam ellipse with an area (emittance) of 6π mm-mrad in which the particles are uniformly distributed. In the second case, the coordinates of the individual particles in the injected beam are selected randomly. A random-number generator was used to select the injection phase ϕ_0 in the range $\pm\pi$. Beam dynamics calculations for the injection beam transport system[7] were used to determine the beam parameters in the interaction region. A Gaussian random-number generator with a standard deviation equal to the electron beam radius (0.054 cm) was used to select the r_m coordinate of the electron. A Gaussian random-number generator with a standard deviation equal to the angular beam divergence (5.36 mrad) was used to select the θ_m coordinate of the electron, where θ_m is the angle the electron trajectory makes with the z-axis. The initial transverse momentum (P_r) of the electron is then given by

$$P_r = \theta_m P_z \qquad (50)$$

where the total momentum of the electron P is given by $P^2 = P_r^2 + P_z^2$.

Figure 21 (a) shows the input and output beams, where the particles are distributed uniformly in phase space. The output beam ellipse has been shifted along the horizontal co-ordinate axis in order to distinguish it from the input beam ellipse. The input phase angle $\xi = 95°$. Figure 21 (b) shows the corresponding output energy spectrum for this case. In Fig. 21 (a) the vertical input beam ellipse is rotated through approximately 45°, but the envelope of the output beam can be approximated to an ellipse.

Figure 22 (a) shows the input and output beams for an input phase angle $\xi = 105°$, and Fig. 22 (b) shows the corresponding output energy spectrum. The output beam emittance is no longer an ellipse, and shows considerable structure about a central lobe. The structure is due to the non linear behaviour of the radial fields and the convolution of the focusing and defocusing forces with phase.

Figures 23 and 24 show the input and output beam profiles for the second case, where the particles were randomly distributed with the phase angle $\xi = 90°$ (in Fig. 23) and ξ uniformly

distributed between $\pm\pi$ (in Fig. 24). The output beam profiles in both these cases show considerable structure, which reflects the non-linear nature of the radial fields. We have examined in some detail the behaviour of various regions of the beam ellipse and the effect on the radial fields in transforming the input beam to the observed output beam profile, although no simple analytical picture can be given.

3 CONCLUSIONS

In this report we have discussed the results of a study of electron acceleration by relativistic large-amplitude electron plasma waves. Although particular reference is made to the laser plasma beatwave concept, the study is equally relevant to the acceleration of particles in the plasma wakefield accelerator and the laser wakefield accelerator concepts. A number of interesting features in the acceleration process have been observed and investigated. There is a threshold energy for the injection of electrons in a large-amplitude electron plasma wave with a phase velocity close to the speed of light. If an incoming electron is moving too slowly with respect to the plasma wave, then the plasma wave outruns the particle before it can experience any acceleration. If, on the other hand, the incoming electron is moving too fast with respect to the plasma wave, then it outruns the wave, and once again experiences no acceleration. Hence there is a minimum and maximum injection energy of the electron in which the electron is trapped by the plasma wave. The threshold energy for particle trapping is increased for a spatially non-uniform plasma wave amplitude, as would be the case for a focused laser beam. Higher injection is required for amplitude-modulated waves than would be the case for plane waves. For maximum energy gain, the system length should be matched to the dephasing length, so that the particle is extracted at the point of maximum energy gain. The longitudinal and radial electric fields are $\pi/2$ out of phase, so that only a small region of the accelerating cycle is useful. Particles should be injected in the accelerating and focussing cycle of the fields. Since current experiments have little control over the injection phase, a spectrum of final electron energies can be expected.

4. REFERENCES

1. T. Tajima and J.M. Dawson, Phys. Rev. Lett. **43**, 267 (1979).
2. P. Chen, J.M. Dawson, R.W. Huff and T. Katsouleas, Phys. Rev. Lett. **54**, 693 (1985).
3. P. Sprangle, E. Esarey, A. Ting and G. Joyce, Appl. Phys. Lett. **53**, 2146 (1988).
4. N.A. Ebrahim, Physics in Canada **45**, 178 (1989).
5. N.A. Ebrahim, Research Trends in Physics (American Institute of Physics), November 1991.
6. F.F. Chen, Introduction to Plasma Physics and Controlled Fusion, 2nd ed., Vol. 1, Plenum (1984).
7. M.N. Rosenbluth and C.S. Liu, Phys. Rev. Lett. **29**, 701 (1972).
8. S.J. Karttunen and R.R.E. Salomaa, Phys. Rev. Lett. **56**, 604 (1986).
9. P. Gibbon and A.R. Bell, Phys. Rev. Lett. **61**, 1599 (1988).
10. P. Mora, Rev. Phys. Appl. **23**, 1489 (1988).
11. C.M. Tang, P. Sprangle and R.N. Sudan, Phys. Fluids **28**, 1974 (1985).
12. J.P. Matte, F. Martin, N.A. Ebrahim, P. Brodeur and H. Pepin, IEEE Trans. Plasma Sci. **PS-15**, 173 (1987).
13. J.D. Lawson, Rutherford Appleton Laboratory, Chilton, Didcot, U.K., Rep. **RL-83-057**, (1983) Unpublished.
14. R. Fedele, U. de Angelis and T. Katsouleas, Phys. Rev. A **33**, 4412 (1986).

Table 1

Parameters for Typical Laser Acceleration Experiments

Laser Wavelengths	10.25 μm and 10.59 μm	9.55 μm and 10.55 μm
Resonant Electron Density (n_0)	10^{16} cm^{-3}	10^{17} cm^{-3}
Plasma Frequency (ω_p)	5.69×10^{12}	1.87×10^{13}
Phase Velocity ($\beta_p = v_p/c$)	0.9995	0.995
Lorentz Factor γ_p	32	10
Electron Quiver Velocity (v_0/c)	0.07	0.07
Pulse risetime (τ_r)	250 ps	250 ps
Pulse width (τ)	500 ps	500 ps
Saturation time (τ_s)	130 ps	65 ps
Density Fluctuations ($\delta n/n_0$)	0.24	0.19
Field Gradient	2.4 GeV/m	6.0 GeV/m
Acceleration Length	22 cm	0.7 cm
Injection Energy	5 - 10 MeV	5 - 10 MeV
Maximum Energy Gain	30 MeV	40 MeV
Maximum Output Energy	40 MeV	50 MeV

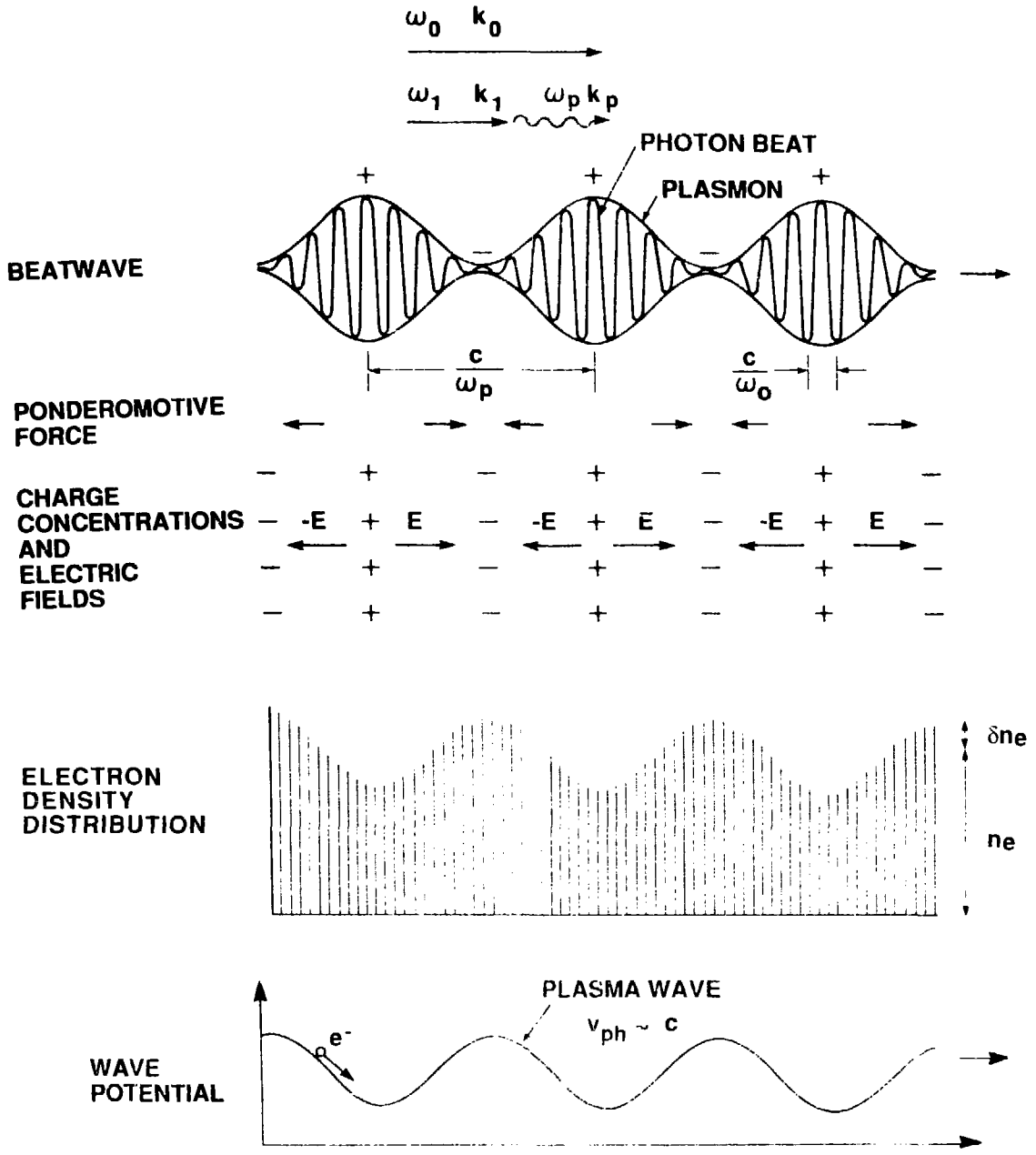

Fig. 1 Schematic diagram of the beatwave, ponderomotive force, concentrations of the positive and negative charges, the associated electric fields, electron density distribution, and the ponderomotive wave in the plasma.

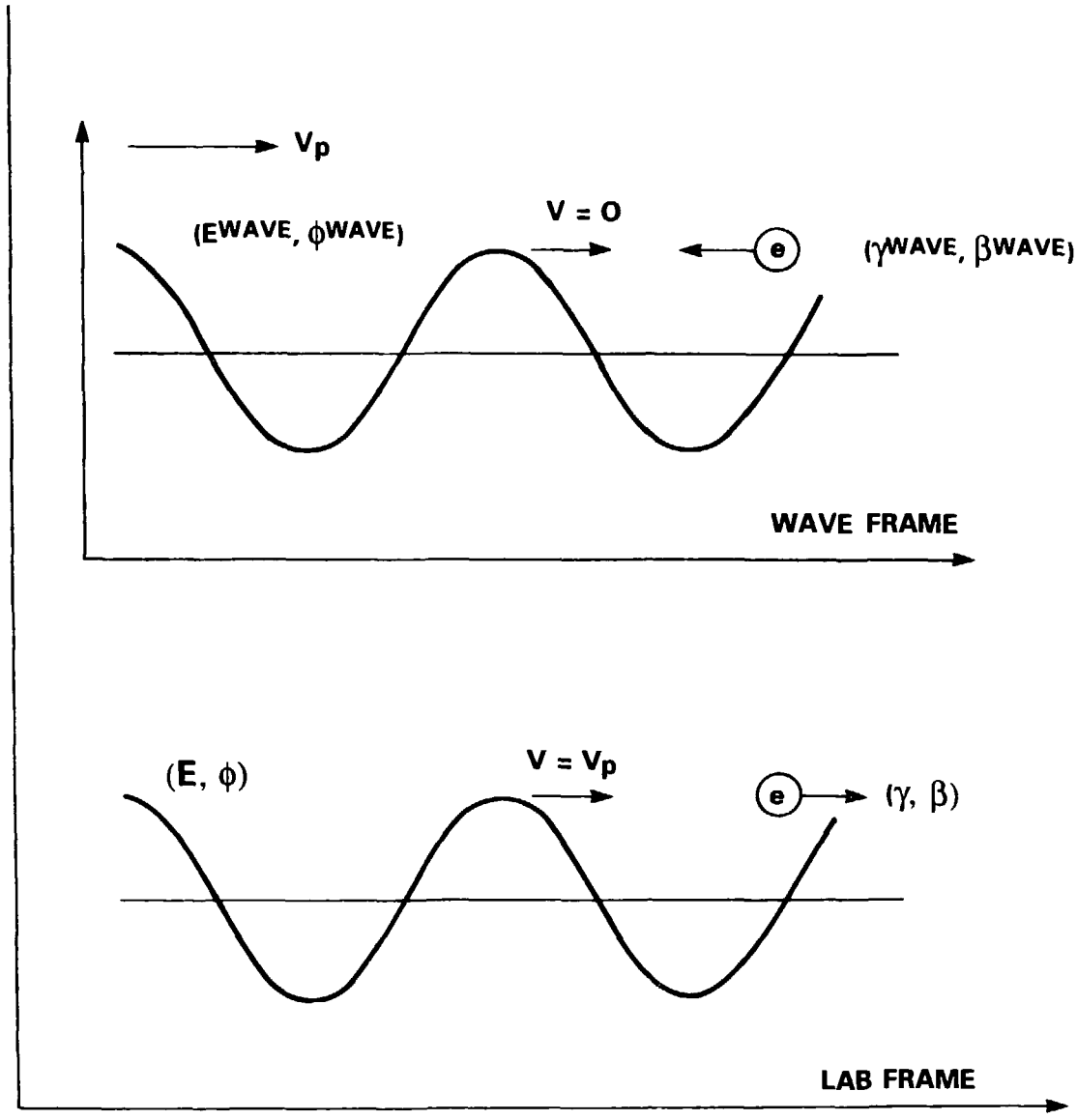

Fig. 2 Relativistic motion of an electron in a large-amplitude plasma wave. The energies and velocities of the electron in the lab and wave frames are given by α, β and γ^{wave}, β^{wave} respectively. The electric field amplitude, the electric potential and the wavenumber for the plasma wave in the lab and wave frames are given by E, ϕ, k_p and E^{wave}, ϕ^{wave}, $k_p{}^{wave}$ respectively. The phase velocities of the plasma wave in the lab and wave frames are v_p and zero respectively.

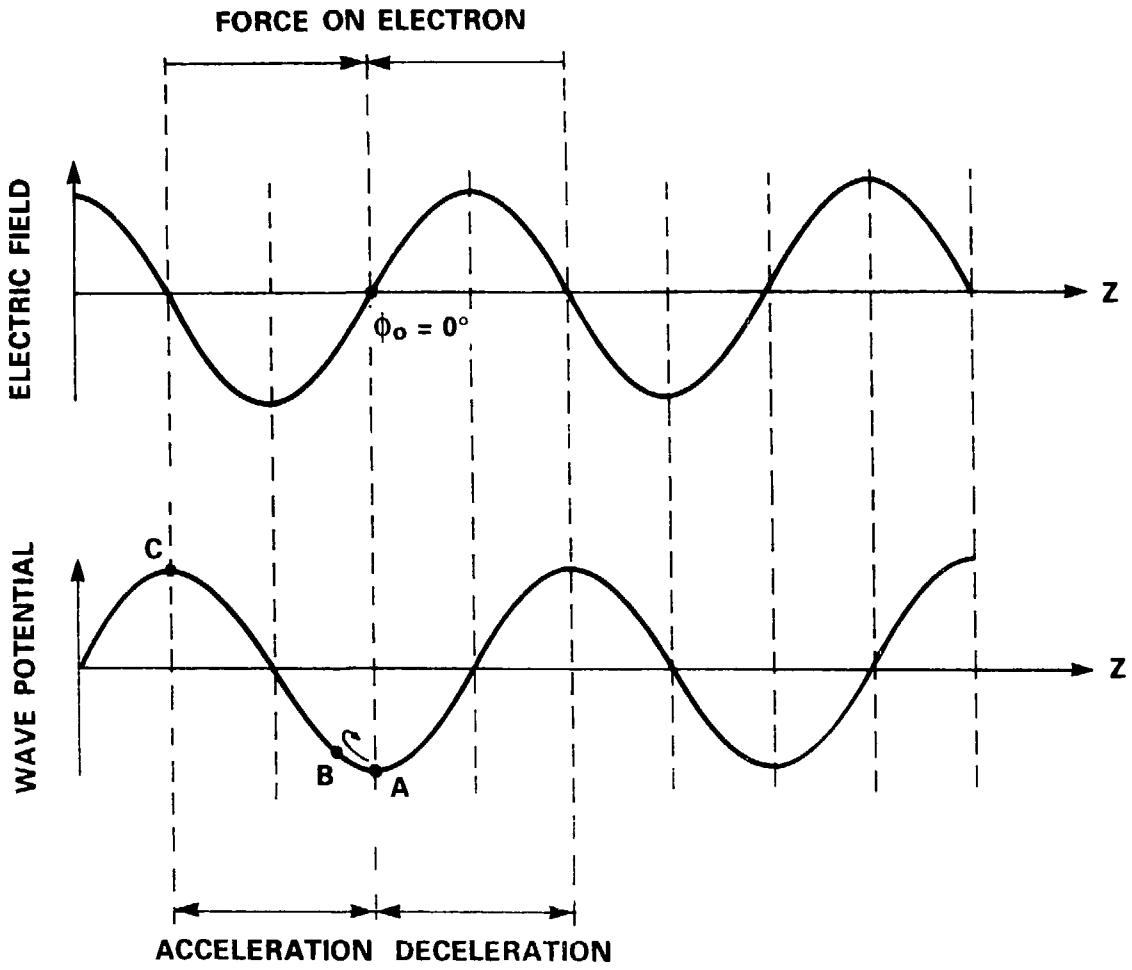

Fig. 3 The electric field and the electric potential of the plasma wave in the wave frame. The accelerating and decelerating forces on the electron are also shown.

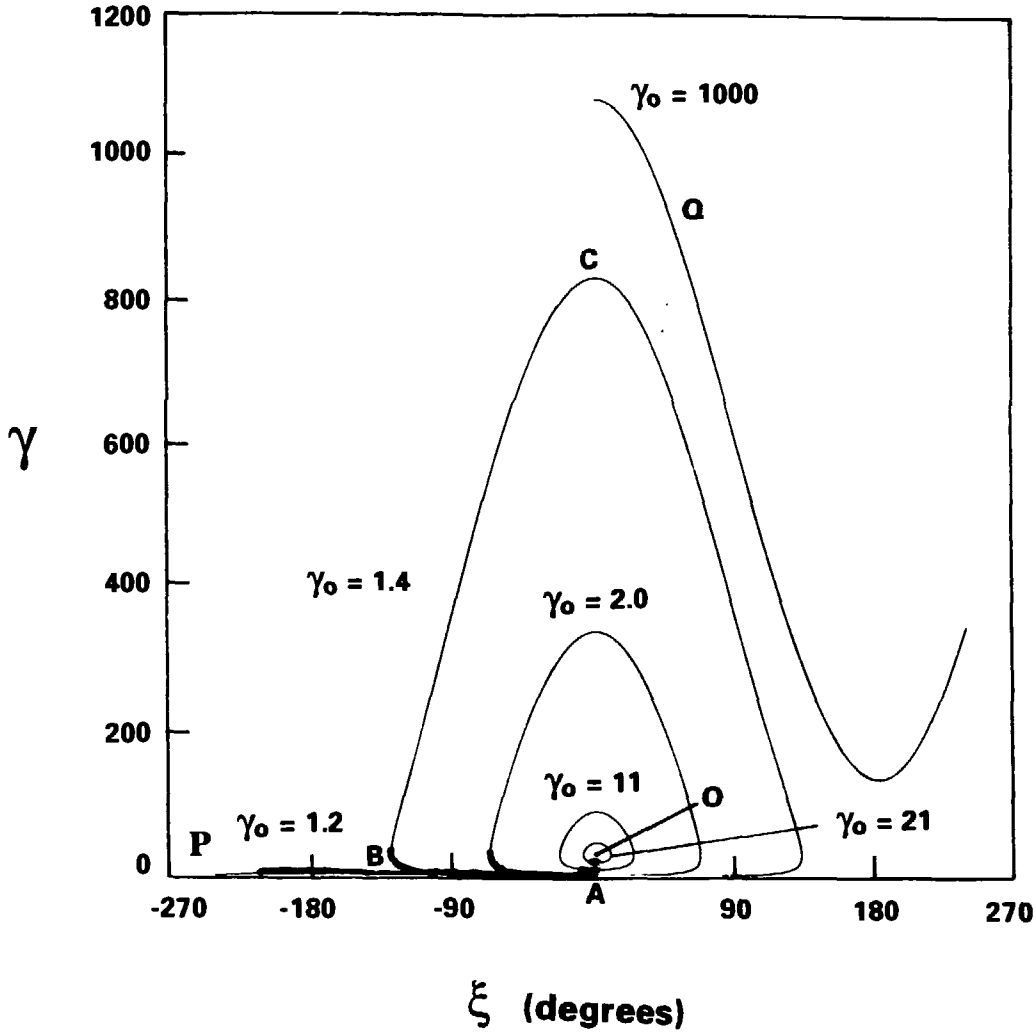

Fig. 4 (a) Particle orbits in phase space (γ, ξ) for particles injected with different initial energies. γ is the lab frame energy and ξ is the wave frame phase. Plasma wave amplitude $\epsilon = 0.24$, wave phase velocity $\beta_p = 0.9995$ and injection phase $\phi_0 = 0°$. Thick lines represent the extent of our experimental system (1.5 cm).

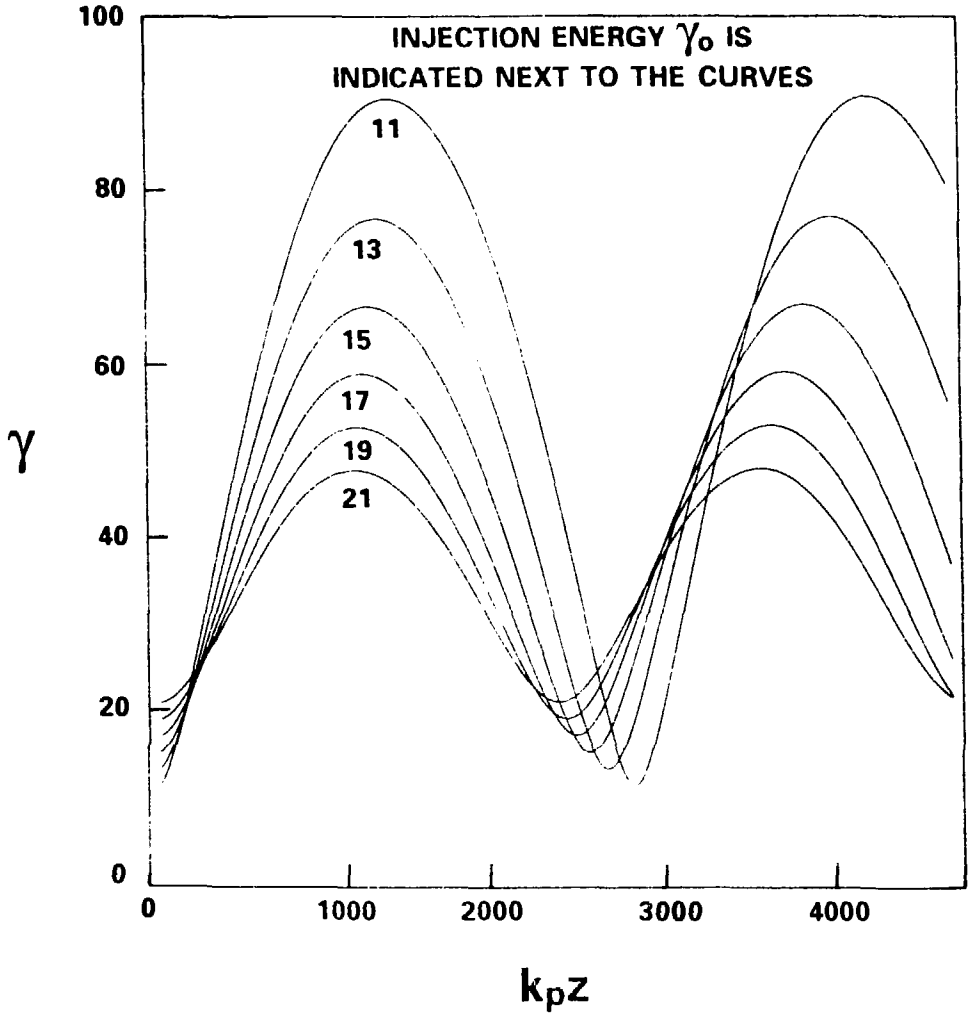

Fig. 4 (b) Variation of electron lab frame energy (γ) with the acceleration distance ($k_pz = z\omega_p/c$), for injection phase $\phi_0 = 0^\circ$, and a set of initial injection energies.

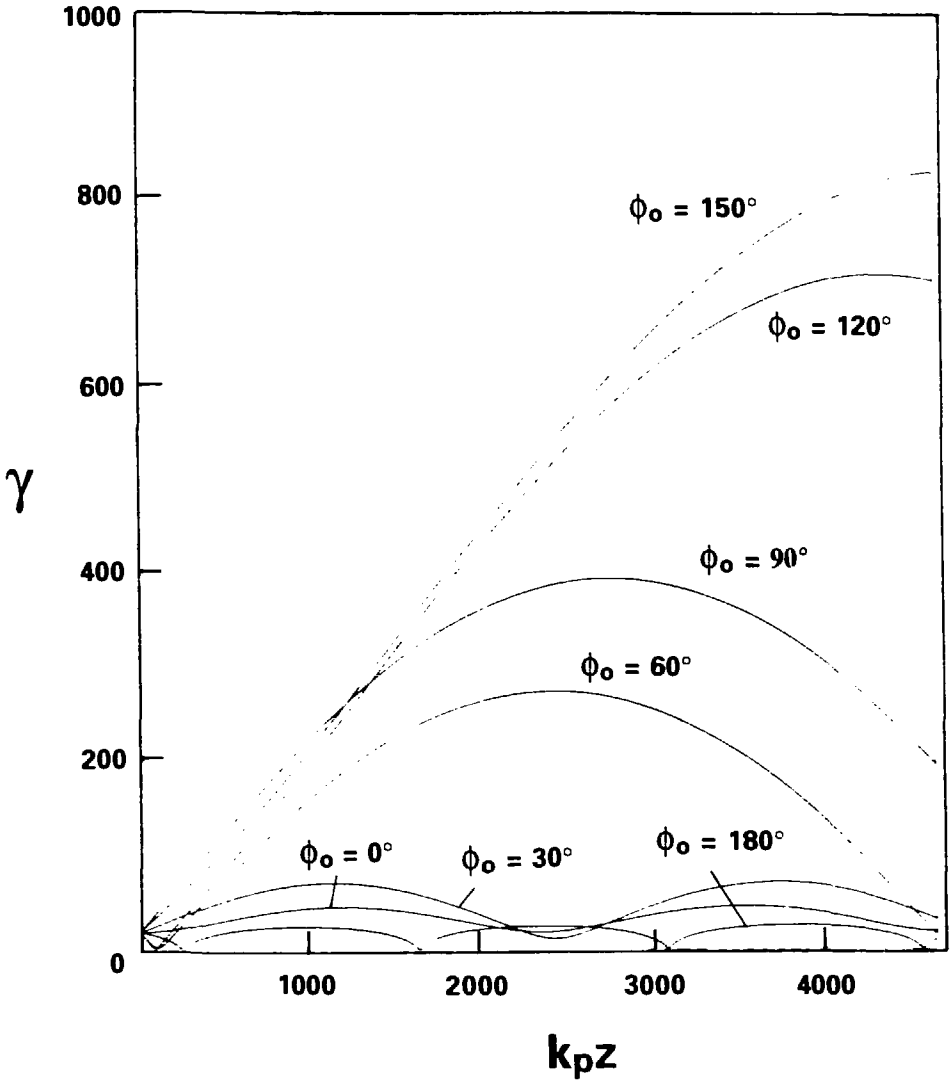

Fig. 4 (c) Variation of electron lab frame energy (γ) with the acceleration distance ($k_p z = z\omega_p/c$), for different values of the injection phase (ϕ_0). Injected electron energy $\gamma_0 = 20$.

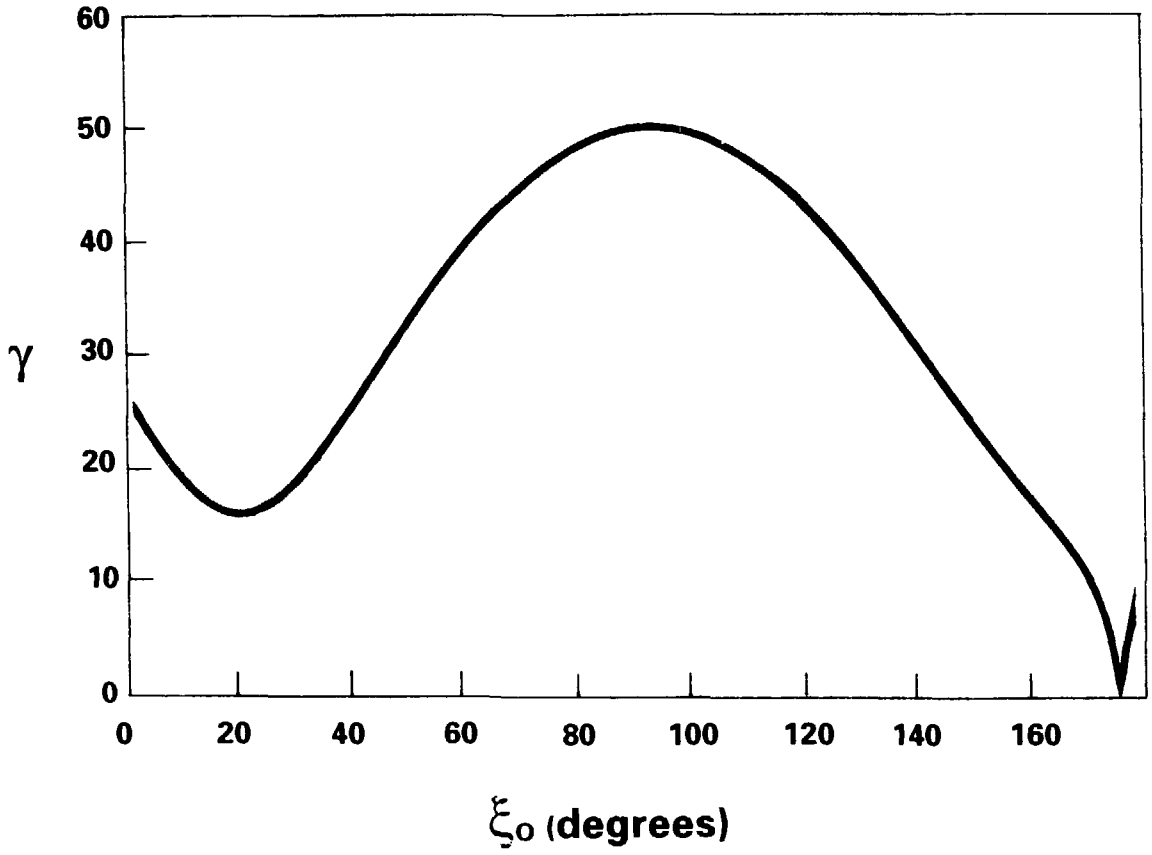

Fig. 4 (d) Spectrum of accelerated electron lab frame energies (γ) for electrons that were injected uniformly in all phases between 0 and π. Injected electron energy $\gamma_0 = 20$.

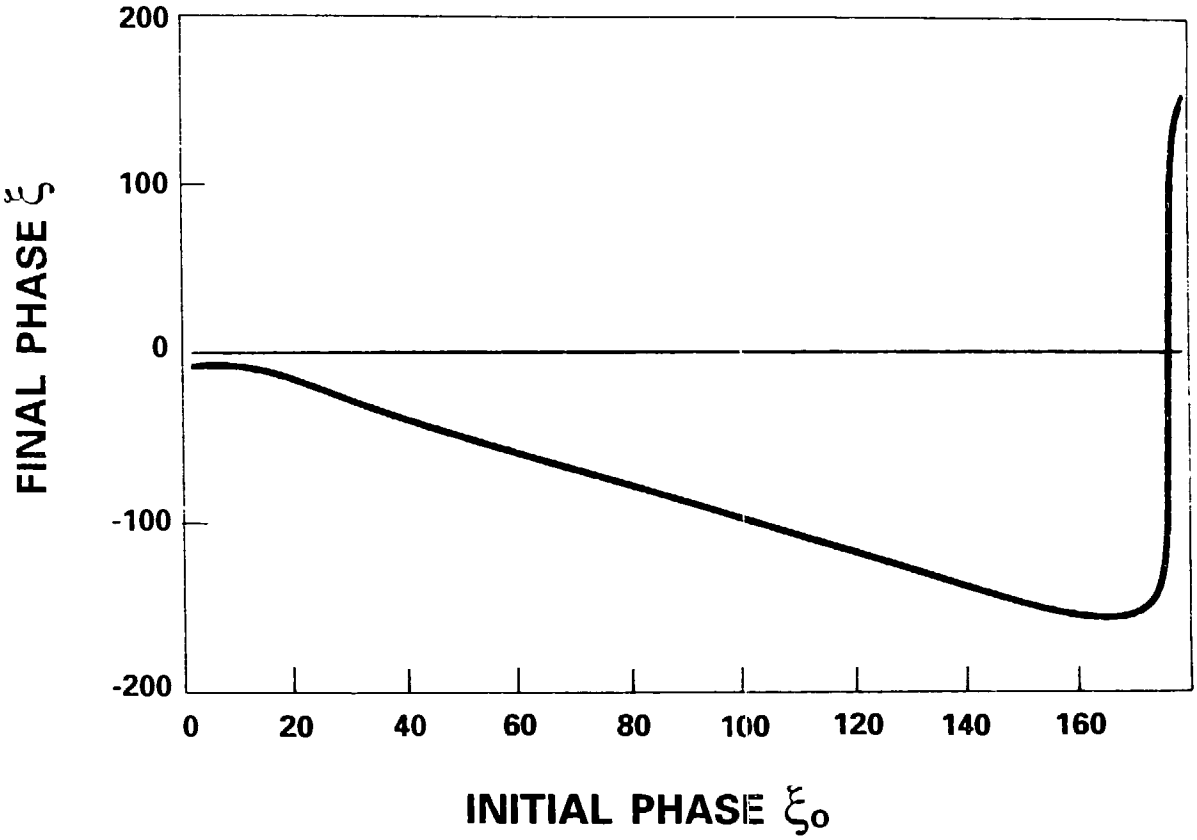

Fig. 4 (c) Distribution of final phases for electrons that were injected uniformly in all phases between 0 and π. Injected electron energy $\gamma_0 = 20$.

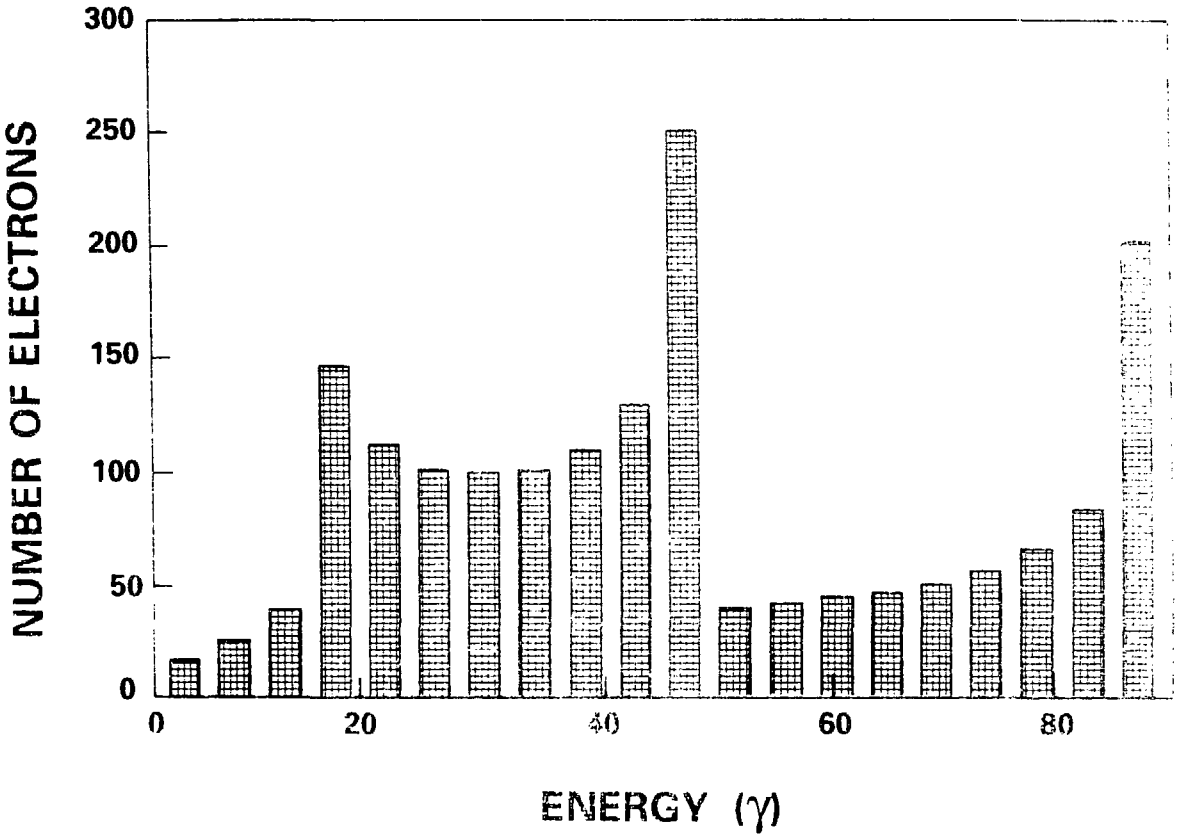

Fig. 4 (f) Accelerated electron energy spectrum for electrons that were injected in phases uniformly distributed between 0 and $\pi/2$. Injected electron energy $\gamma_0 = 20$.

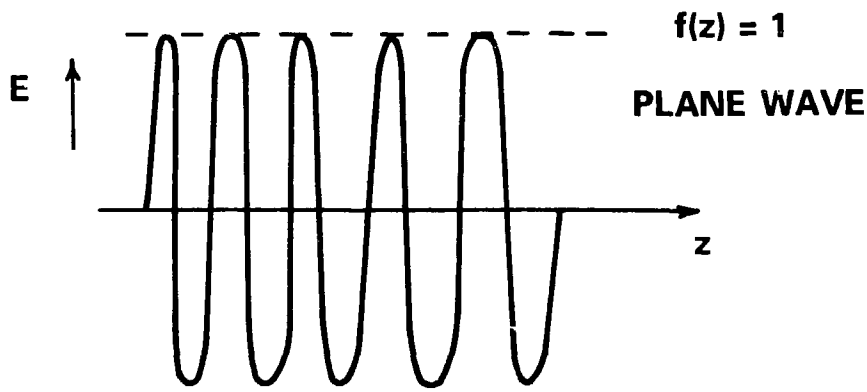

Fig. 5 (a) Spatial profile of the constant-amplitude (plane wave) electric field with f(z) = 1.

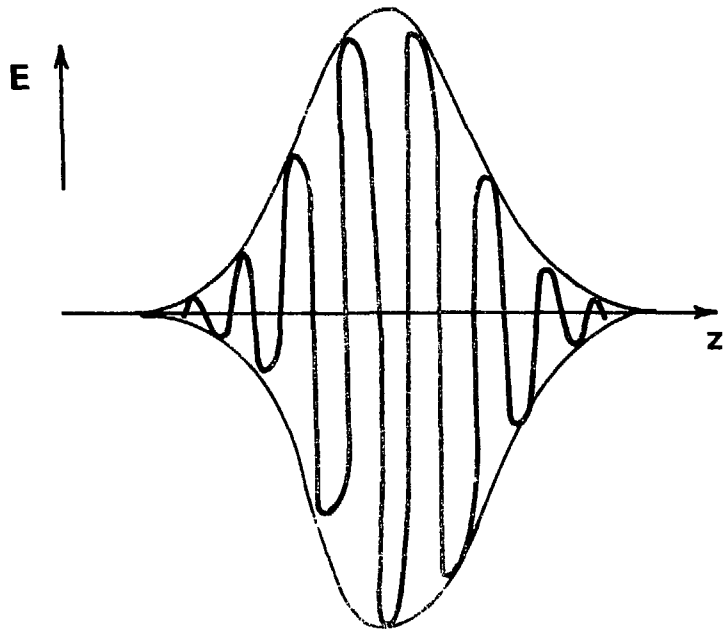

Fig. 5 (b) Spatial profile of the amplitude-modulated electric field.

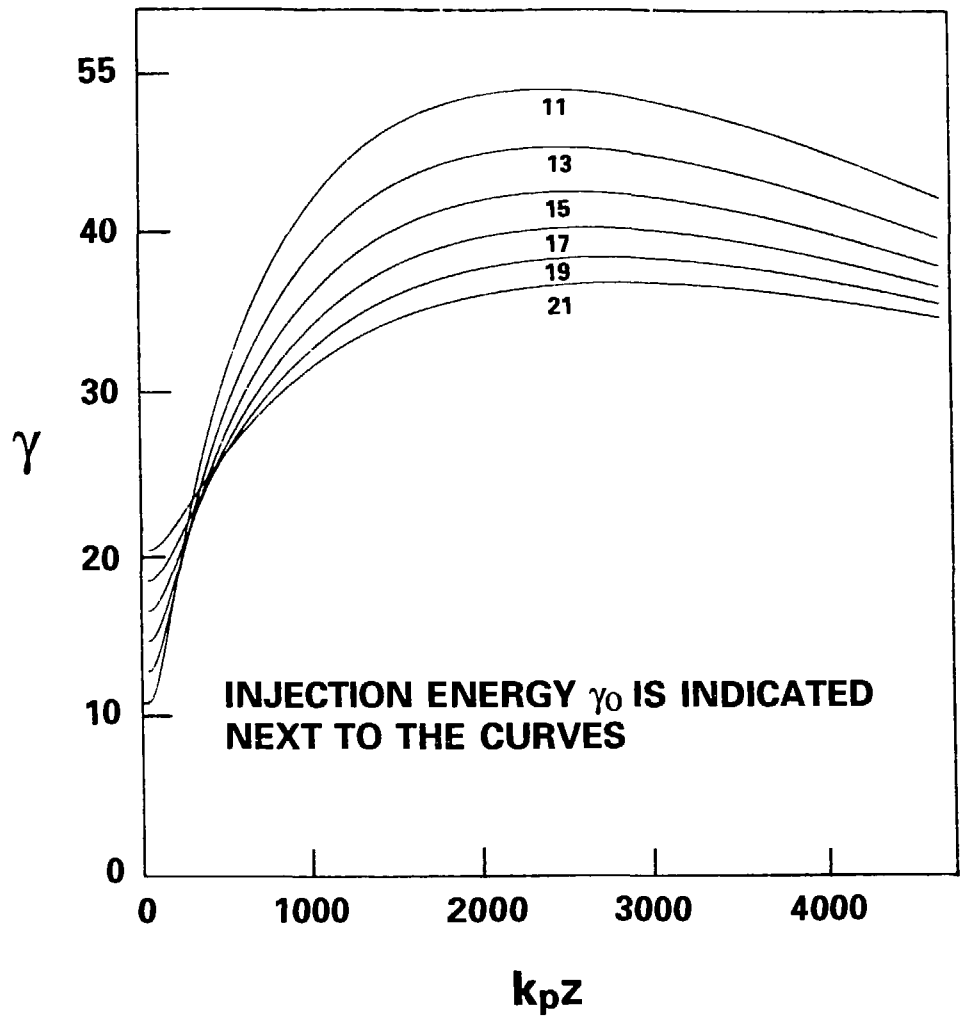

Fig. 6 (a) Variation of electron lab frame energy (γ) with the acceleration distance ($k_p z = z\omega_p/c$), for different values of injection phase energies. Injection phase $\phi_0 = 0°$.

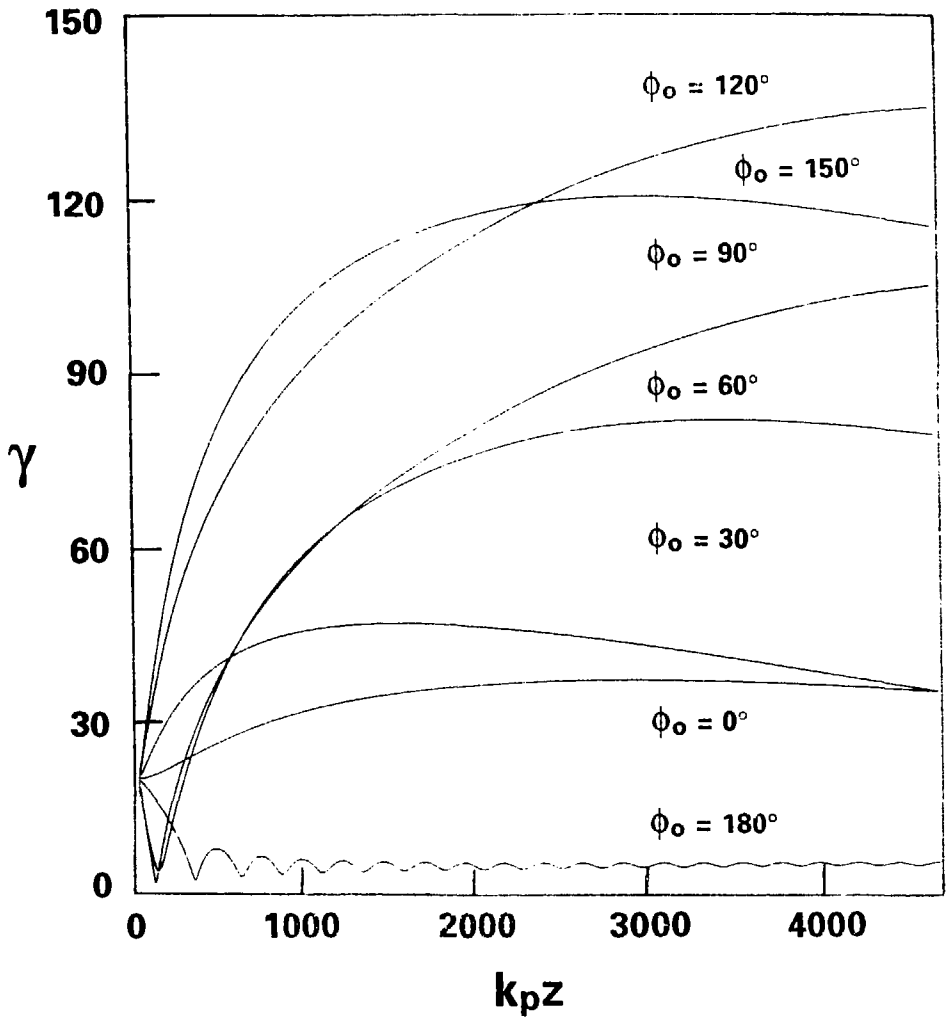

Fig. 6 (b) Variation of electron lab frame energy (γ) with the acceleration distance ($k_p z = z\omega_p/c$), for different values of the injection phase (ϕ_0). Injected electron energy $\gamma_0 = 20$.

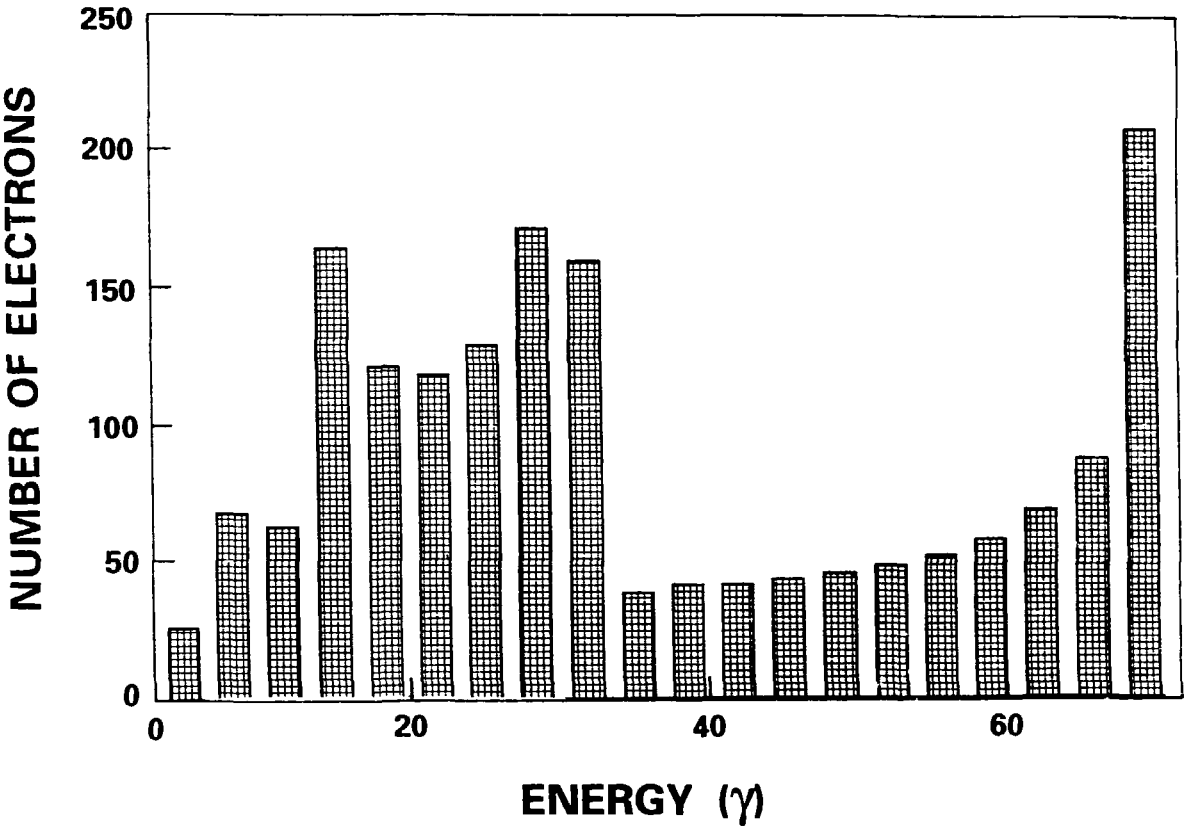

Fig. 6 (c) Accelerated electron energy spectrum for electrons that were injected in phases uniformly distributed between 0 and $\pi/2$. Injected electron energy $\gamma_0 = 20$.

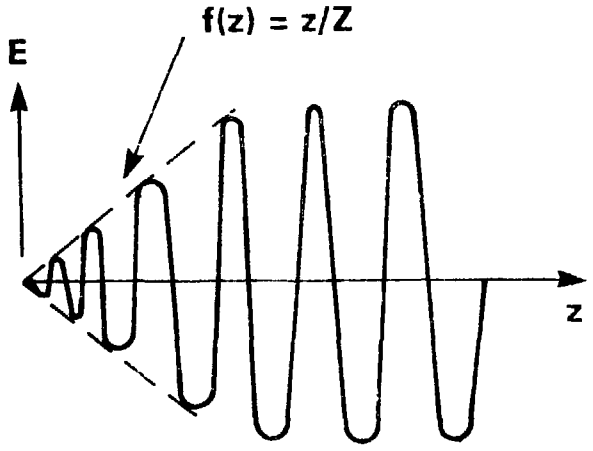

Fig. 7 Spatial profile of amplitude modulated electric field with a linear leading edge f(z) = z/Z.

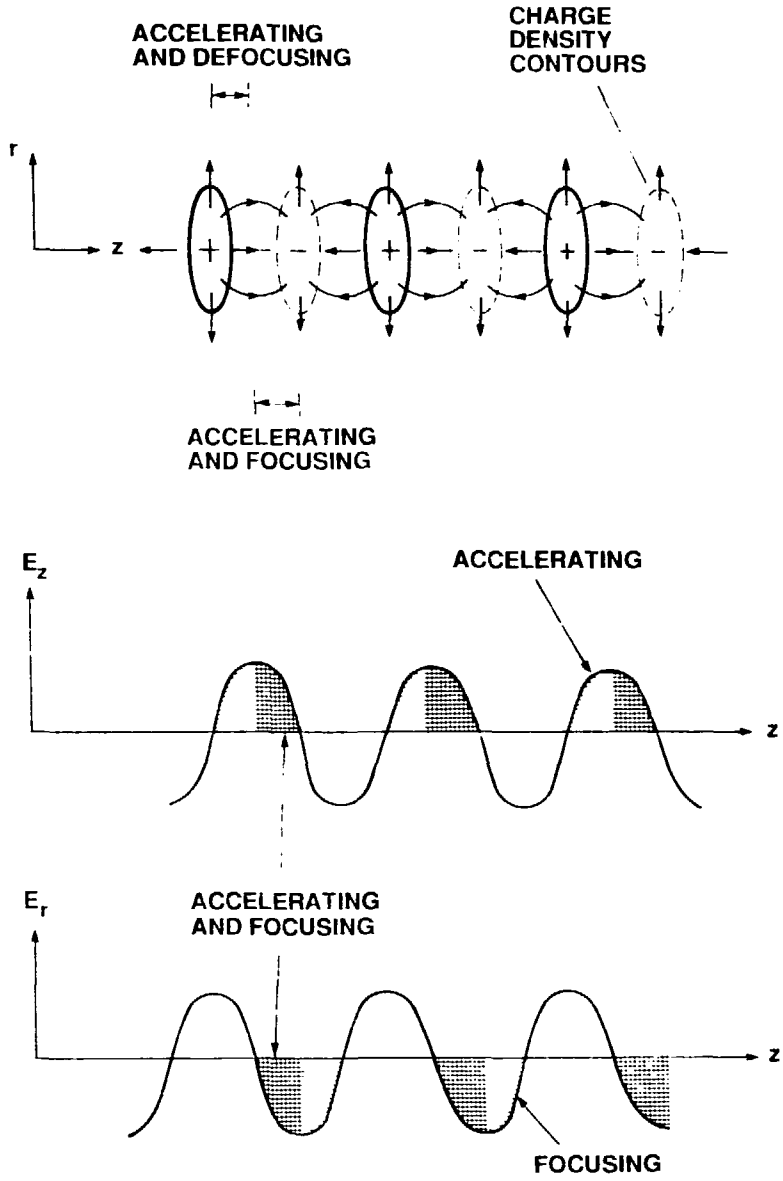

Fig. 8 Charge density contours, axial and radial electric fields in a plasma wave of finite radial dimensions.

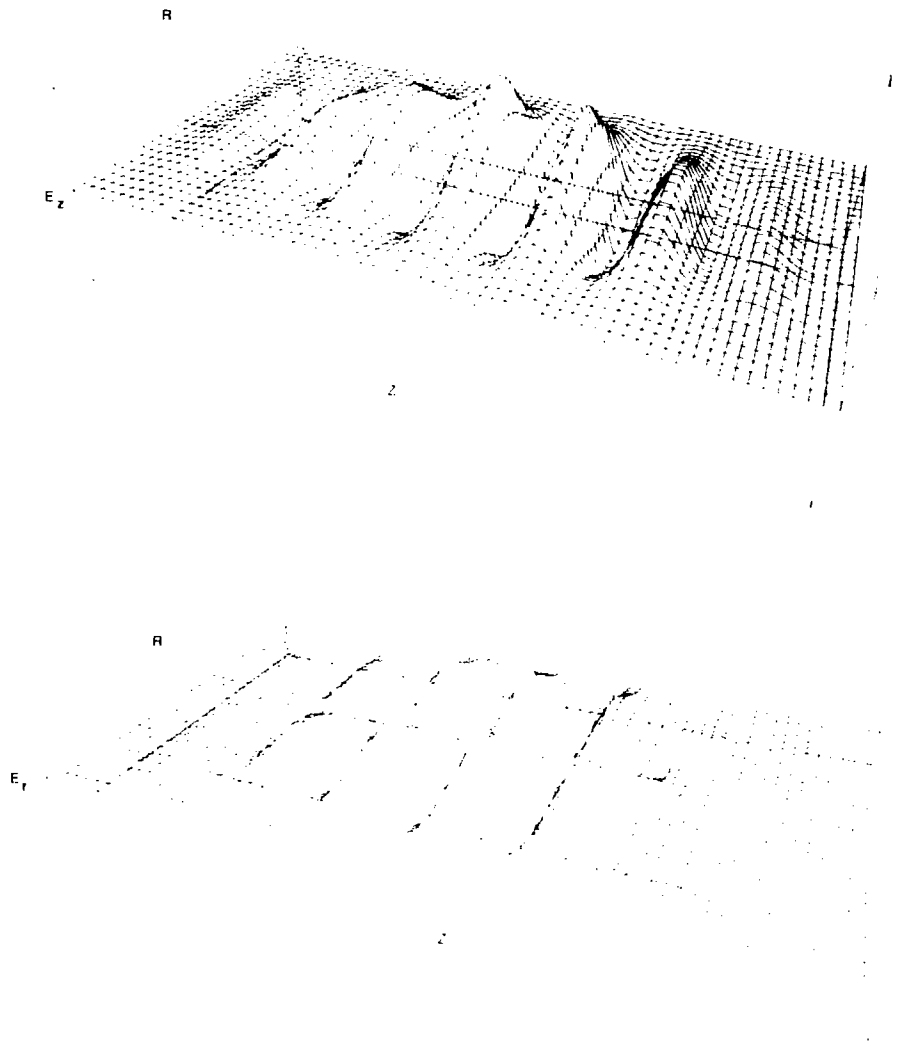

Fig. 9 Profiles of the axial (E_z) and radial (E_r) fields of the plasma waves. The laser axis lies along the axial z-direction.

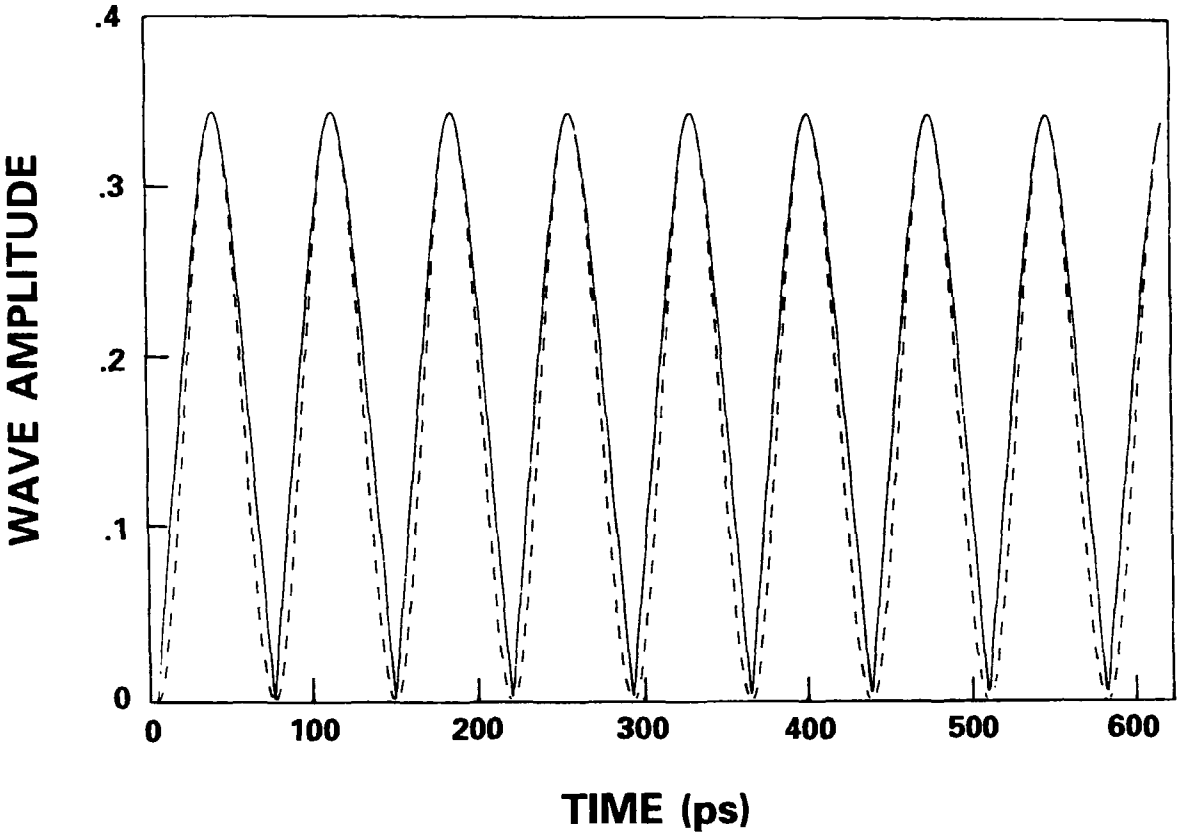

Fig. 10 Variation of plasma wave amplitude ($\epsilon = \delta n_e/n_e$) with time from a one-dimensional, non-linear, fully relativistic model of the plasma wave.

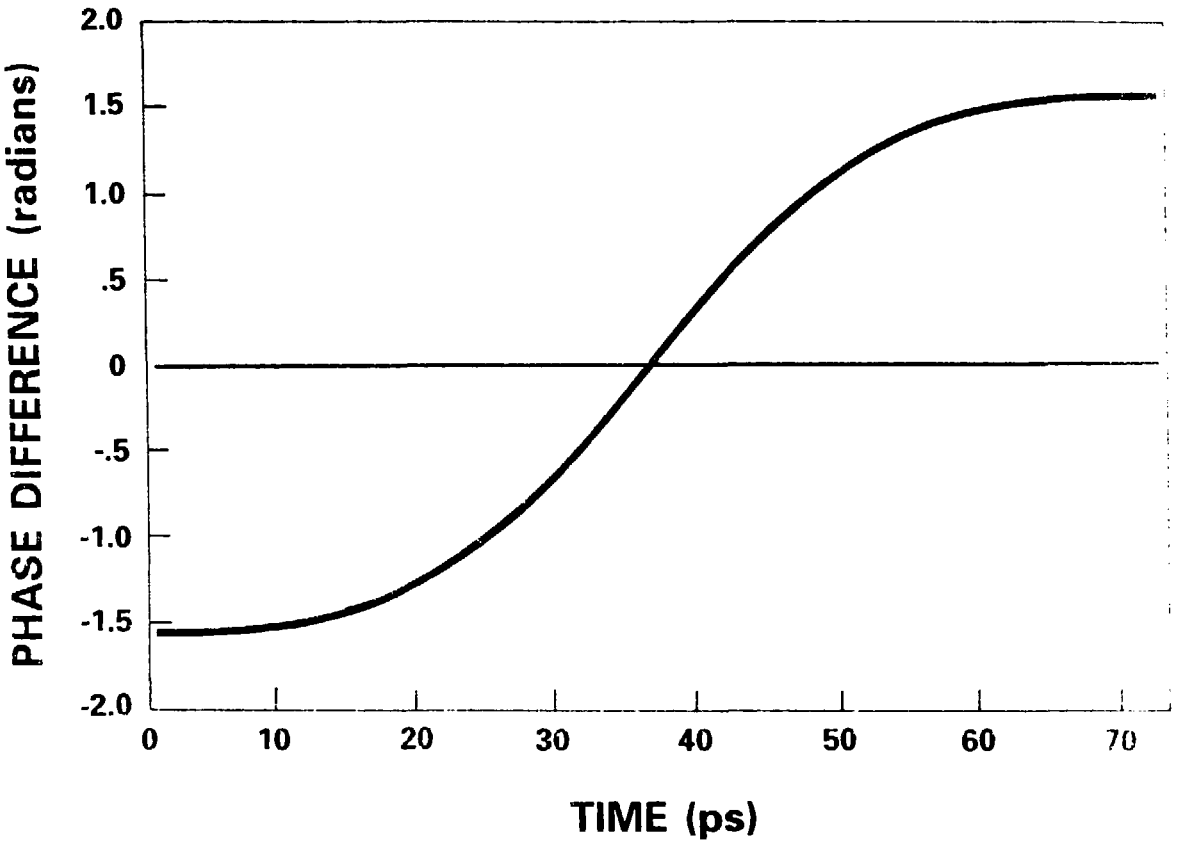

Fig. 11 Variation of the phase difference between the laser driver and plasma wave with time from a one-dimensional, non-linear, fully relativistic model of the plasma wave.

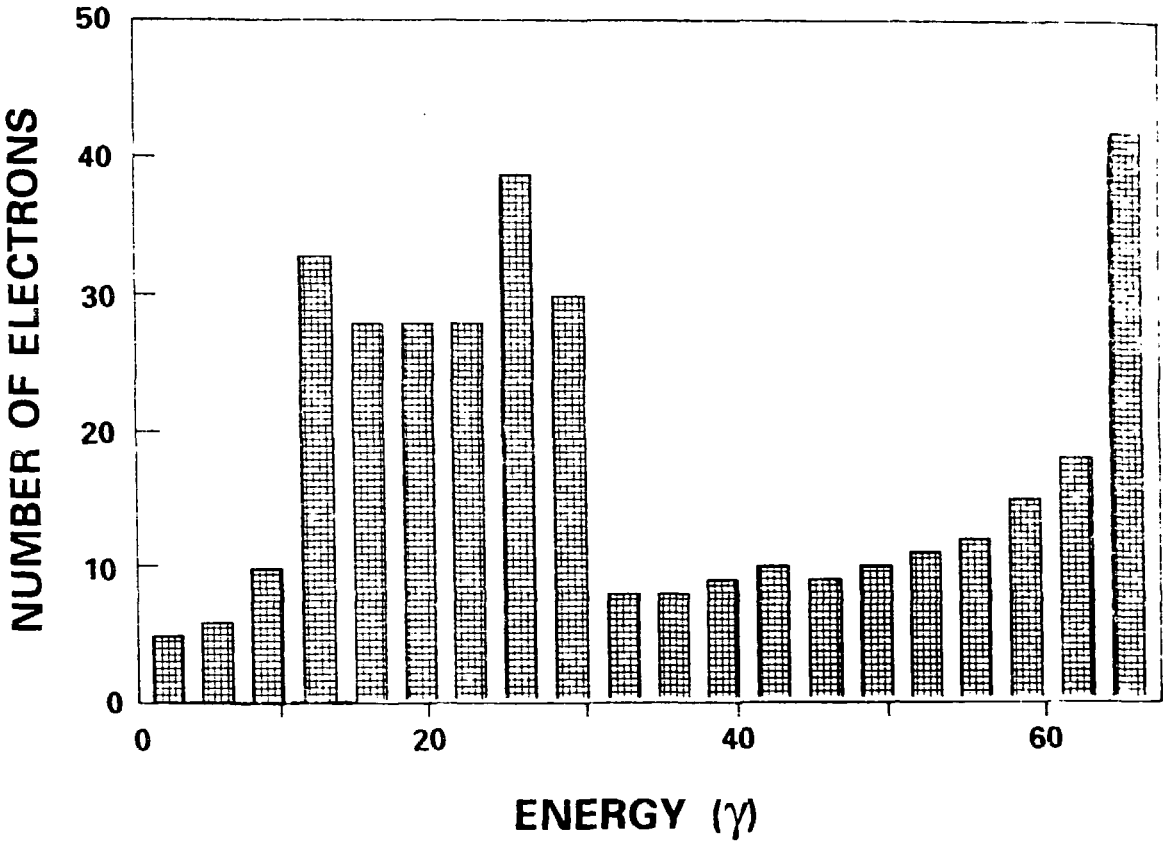

Fig. 12 (a) Accelerated electron energy spectrum from a one-dimensional model with a fixed plasma wave amplitude

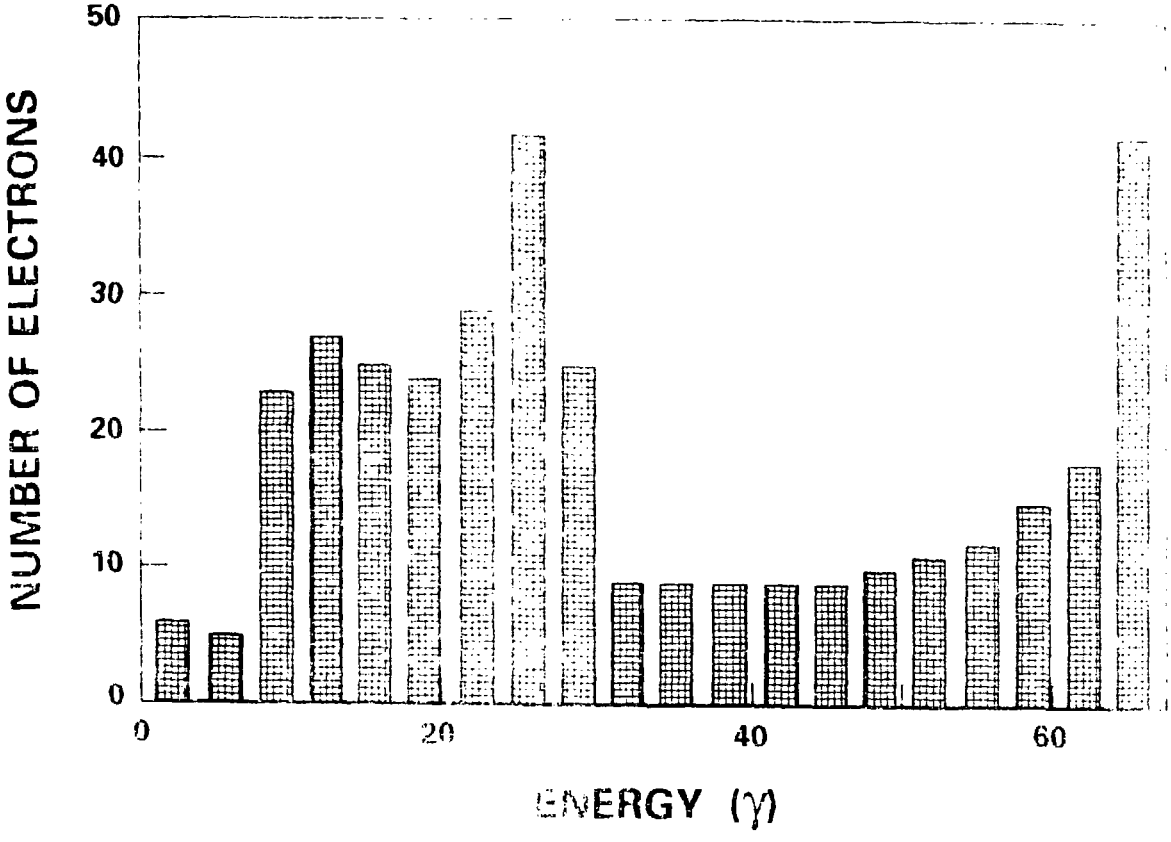

Fig. 12 (b) Accelerated electron energy spectrum from a one-dimensional, non-linear fully relativistic model with a linearly rising plasma wave amplitude.

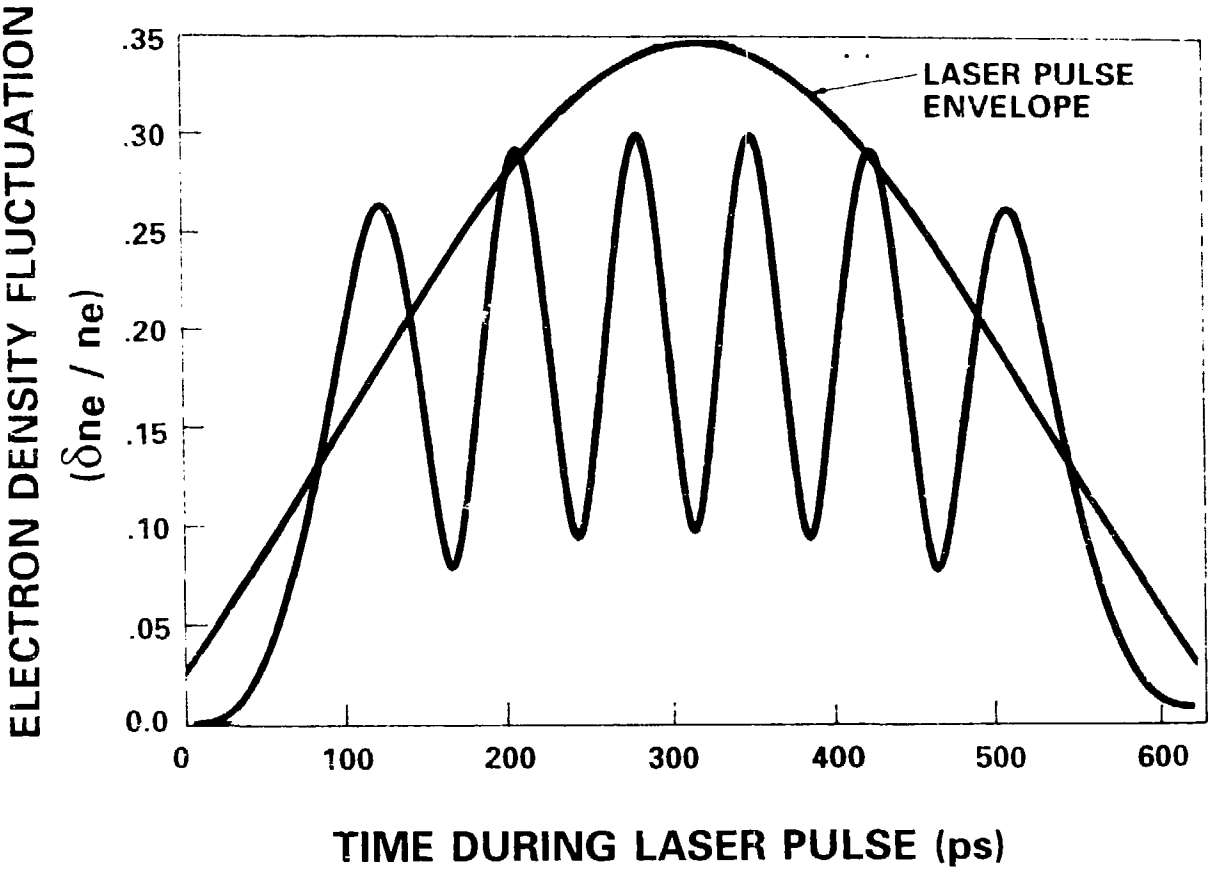

Fig. 13 Variation of plasma wave amplitude (density fluctuation $\delta n_e/n_e$) with time for a finite duration laser pulse. Laser pulse risetime is 250 ps and a full-width-half maximum duration of 500 ps. The laser pulse envelope is shown in this figure.

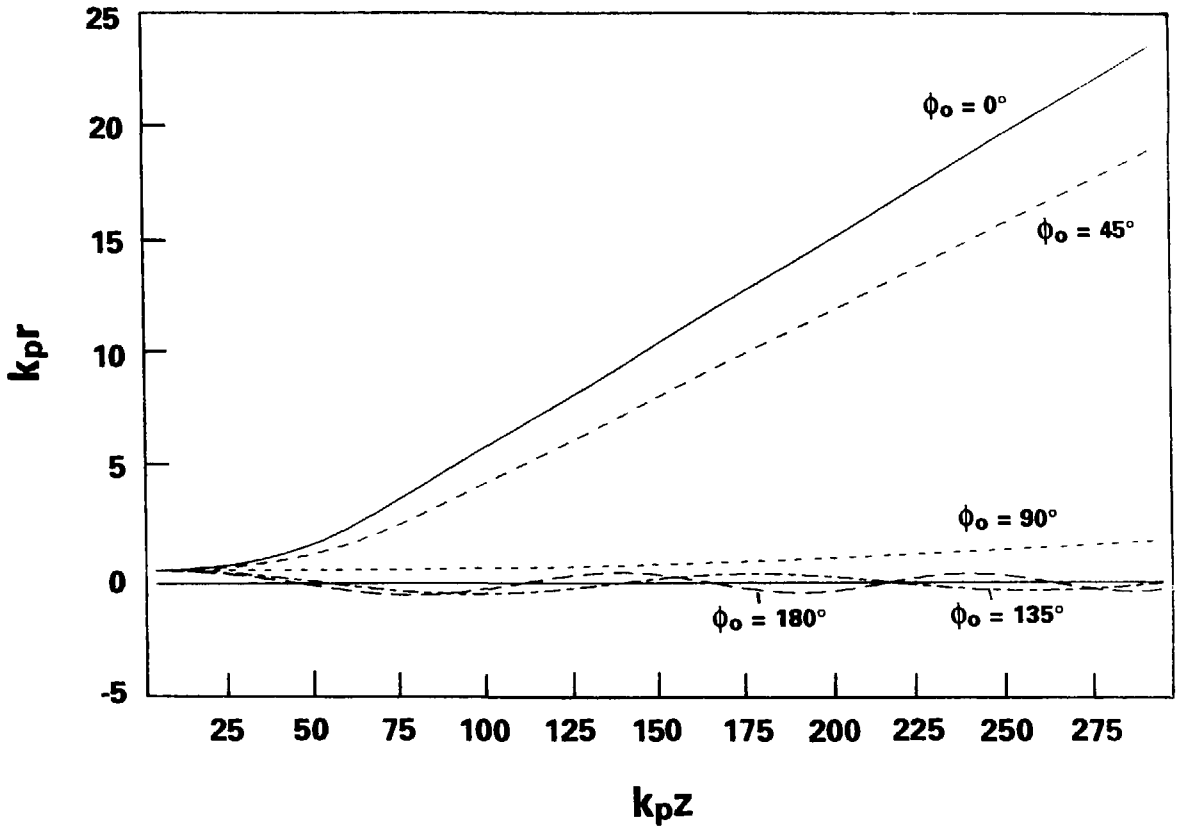

Fig. 14 Trajectories of electrons injected into a two-dimensional plasma wave at the same radial distance ($k_p r = 30$) but with different injection phases. Plasma wave amplitude $\epsilon = 0.24$, wave phase velocity $\beta_p = 0.9995$. Acceleration distance $k_p z = z\omega_p/c$ and radial distance $k_p r = r\omega_p/c$.

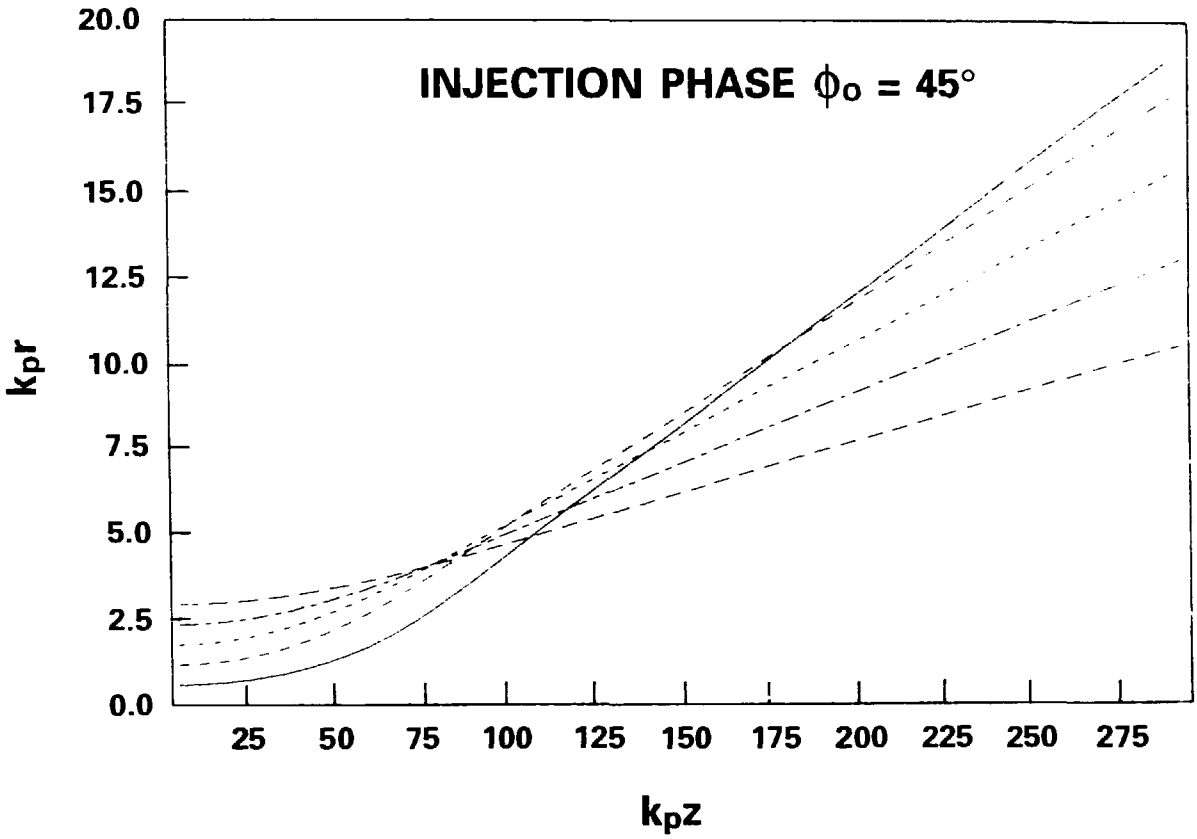

Fig 15 Trajectories of electrons injected into a two-dimensional plasma wave at different radial distances ($k_p r$). Electron injection phase $\phi_0 = 45°$. Plasma wave amplitude $\epsilon = 0.24$, wave phase velocity $\beta_p = 0.9995$. Acceleration distance $k_p z = z\omega_p/c$.

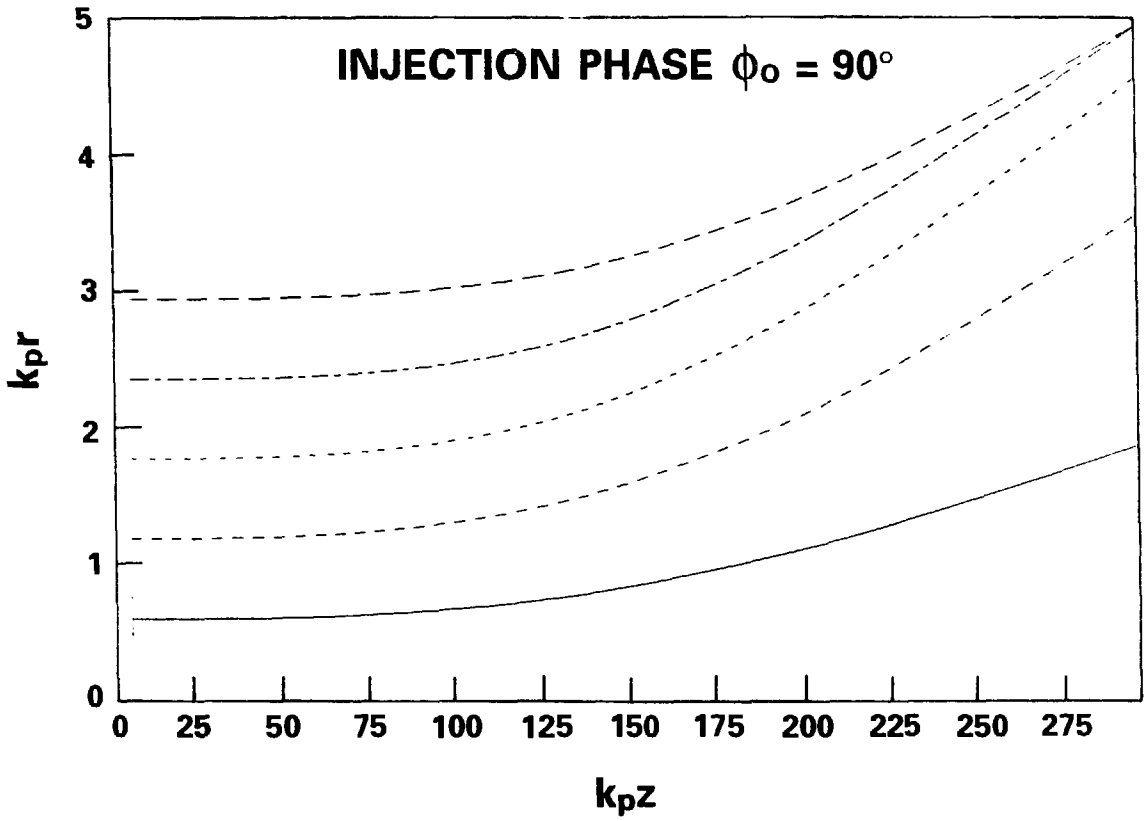

Fig. 16 Trajectories of electrons injected into a two-dimensional plasma wave at different radial distances ($k_p r$). Electron injection phase $\phi_0 = 90°$. Plasma wave amplitude $\epsilon = 0.24$, wave phase velocity $\beta_p = 0.9995$. Acceleration distance $k_p z = z\omega_p/c$ and radial distance $k_p r = r\omega_p/c$.

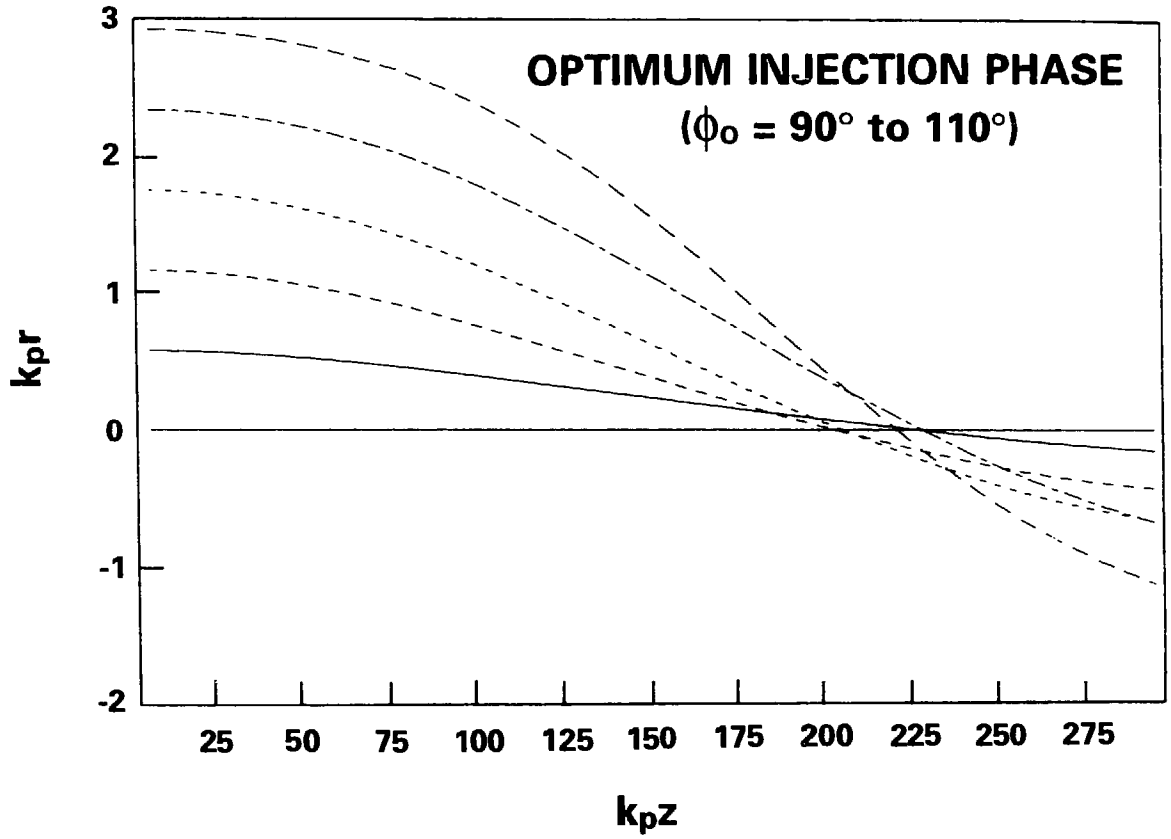

Fig. 17 Trajectories of electrons injected into a two-dimensional plasma wave at different radial distances ($k_p r$). Electron injection phase ϕ_0 is optimized for maximum output electron energy, and lies between 90° and 110°. Plasma wave amplitude $\epsilon = 0.24$, wave phase velocity $\beta_p = 0.9995$. Acceleration distance $k_p z = z\omega_p/c$ and radial distance $k_p r = r\omega_p/c$.

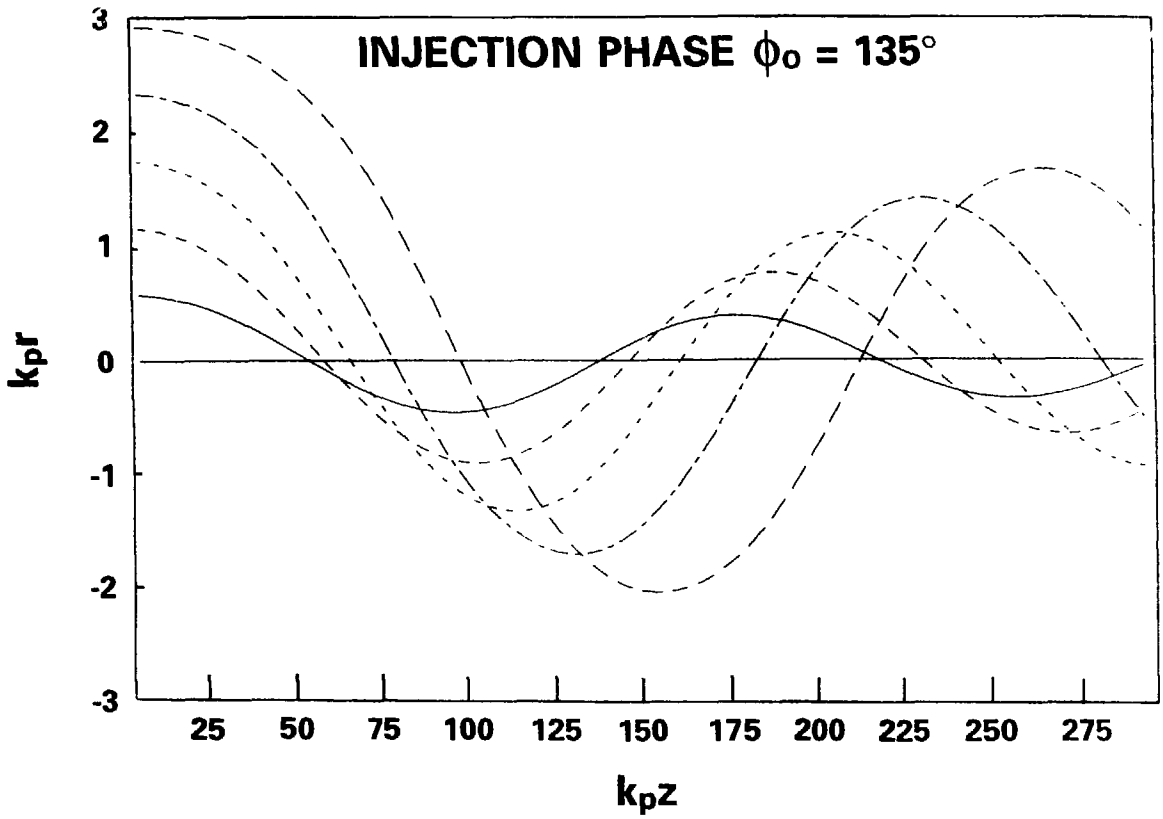

Fig. 18 Trajectories of electrons injected into a two-dimensional plasma wave at different radial distances (k_pr). Electron injection phase $\phi_0 = 135°$. Plasma wave amplitude $\epsilon = 0.24$, wave phase velocity $\beta_p = 0.9995$. Acceleration distance $k_pz = z\omega_p/c$ and radial distance $k_pr = r\omega_p/c$.

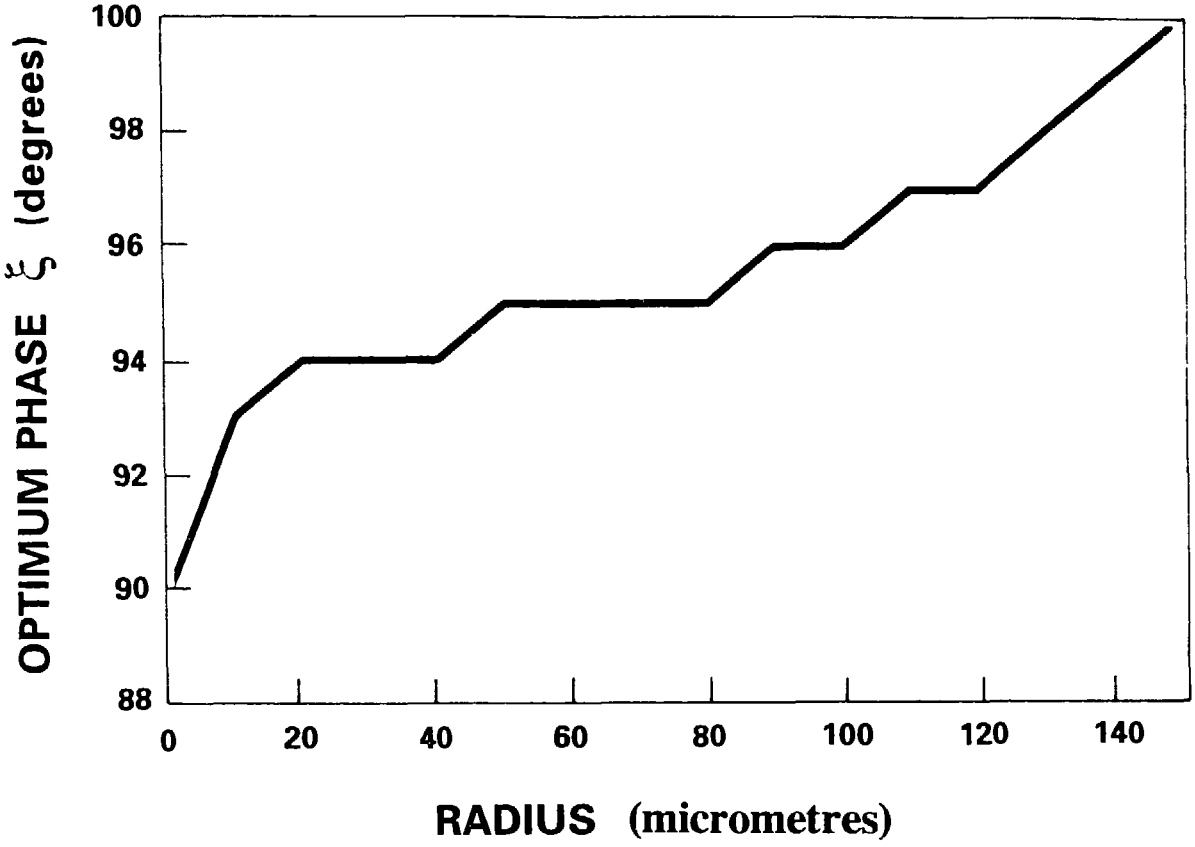

Fig. 19 Variation of optimum phase ξ (optimized for maximum output electron energy) with radius. Plasma wave amplitude $\epsilon = 0.24$, wave phase velocity $\beta_p = 0.9995$.

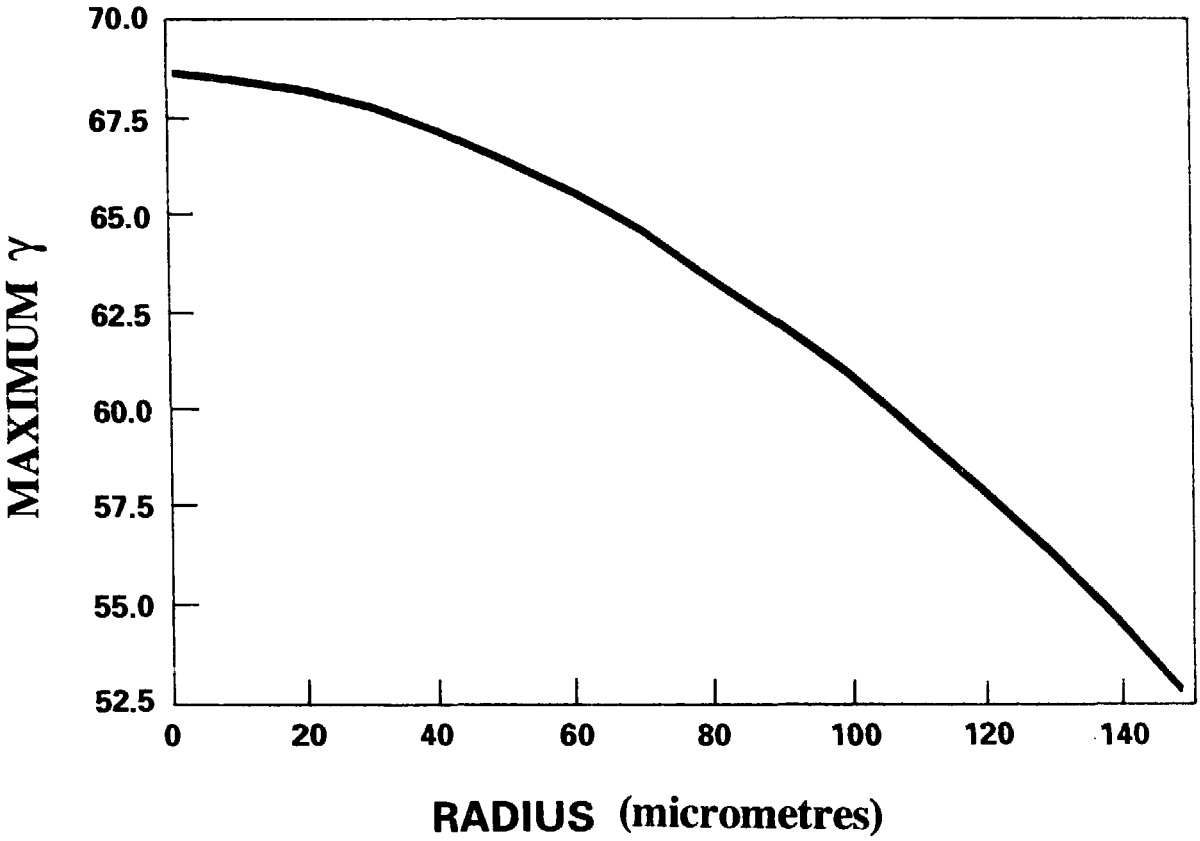

Fig. 20 Variation of maximum output energy of the electron γ with radius. Plasma wave amplitude $\epsilon = 0.24$, wave phase velocity $\beta_p = 0.9995$. Injected electron energy $\gamma_0 = 20$.

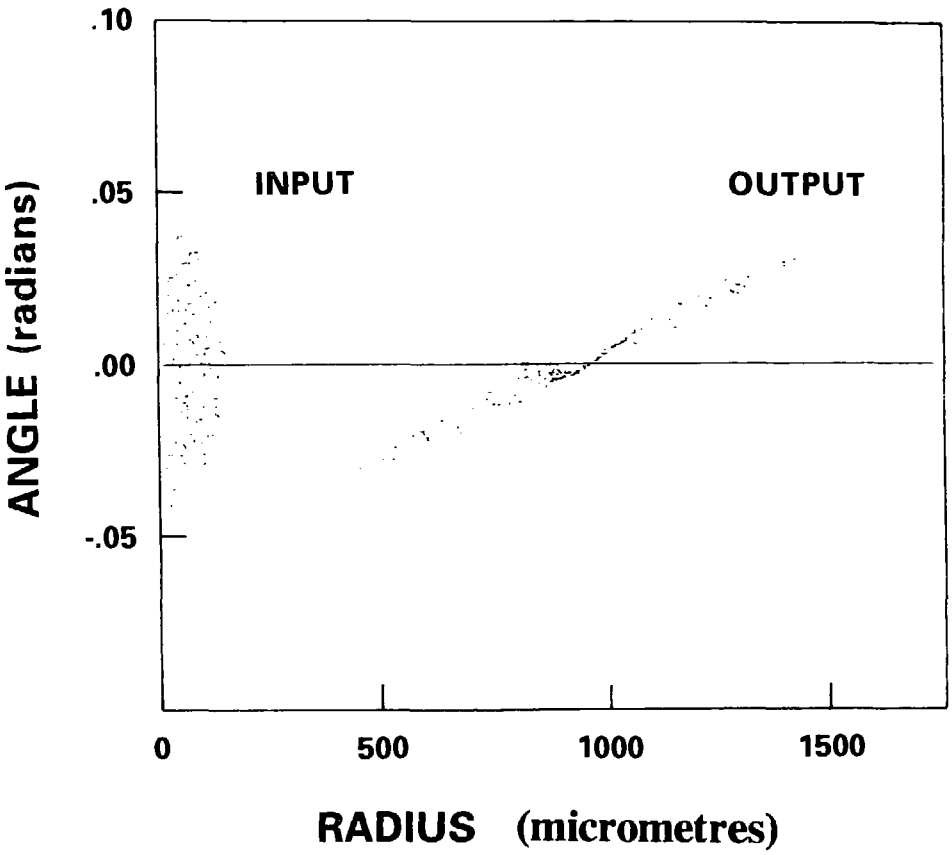

Fig. 21 (a) Radial emittance diagrams at the input (object) and output (image) planes for electrons injected into a two-dimensional plasma wave. Plasma wave amplitude $\epsilon = 0.24$, wave phase velocity $\beta_p = 0.9995$. Injected electron energy $\gamma_0 = 20$. Input phase $\phi_0 = 95°$. Injected electrons were uniformly distributed in phase space. The output beam is shifted along the radial axis for clarity in this figure.

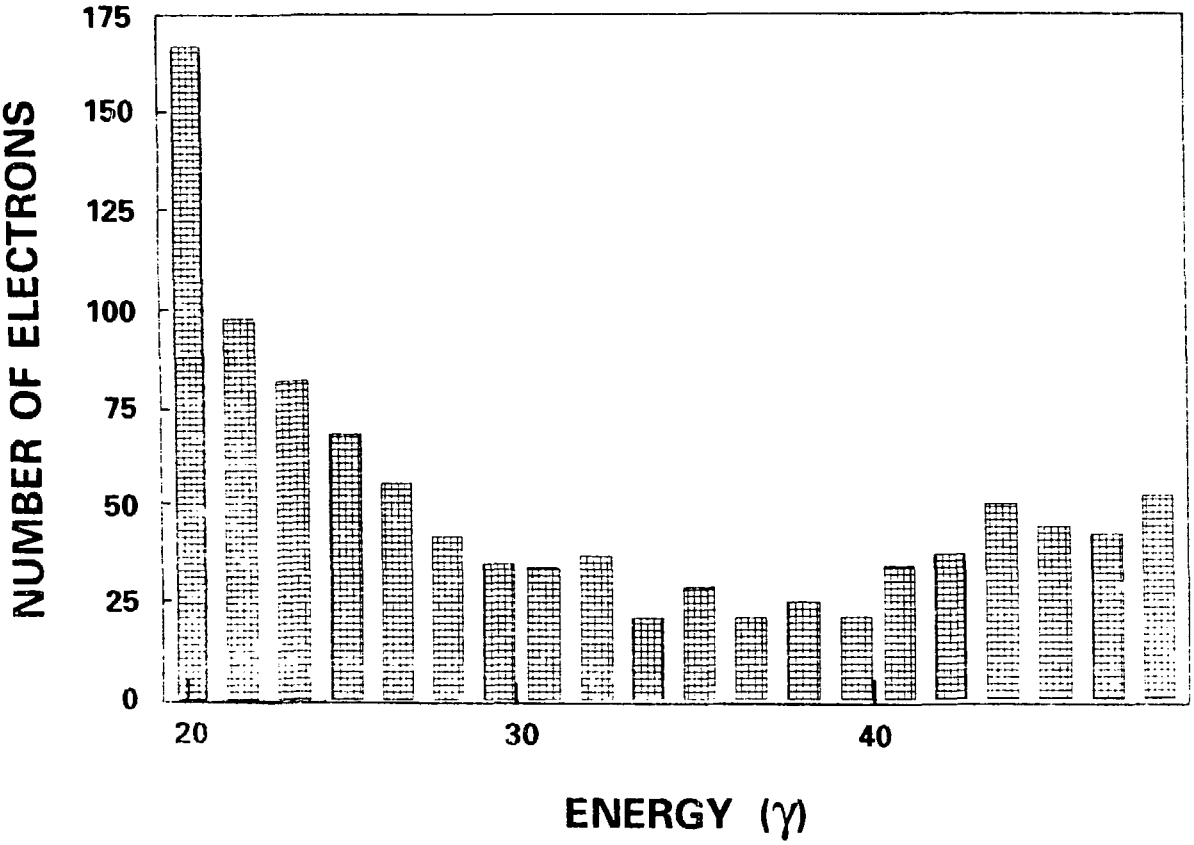

Fig. 21 (b) Accelerated electron energy spectrum for the case shown in Fig. 21 (a).

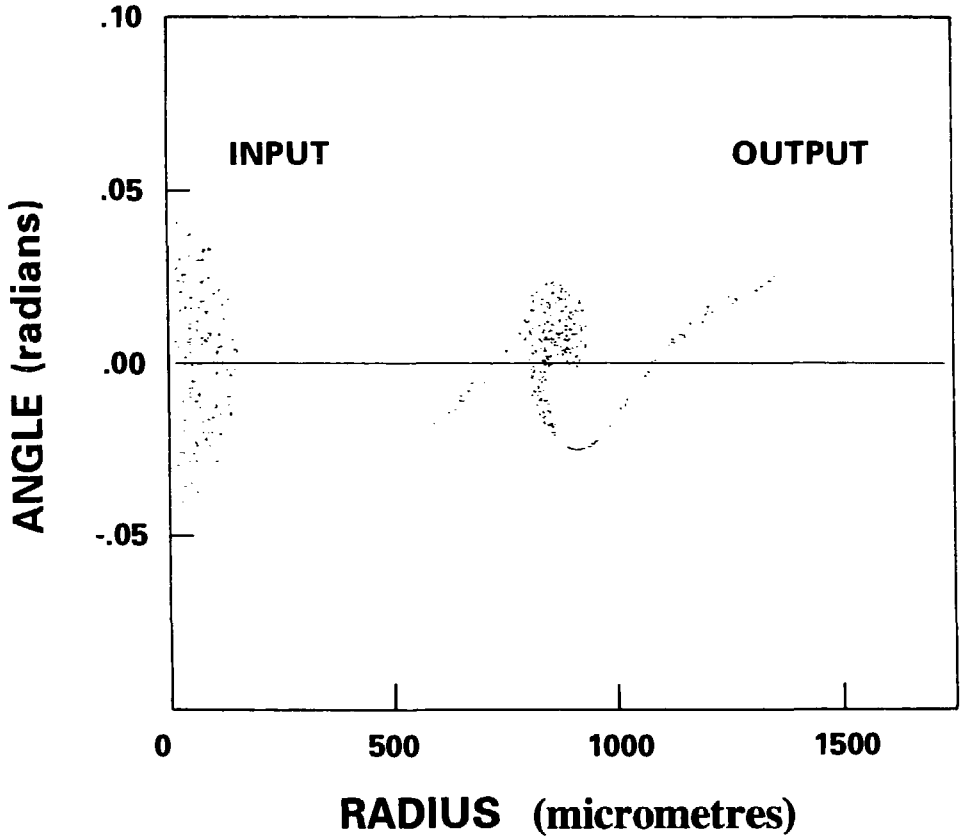

Fig. 22 (a) Radial emittance diagrams at the input (object) and output (image) planes for electrons injected into a two-dimensional plasma wave. Plasma wave amplitude $\epsilon = 0.24$, wave phase velocity $\beta_p = 0.9995$. Injected electron energy $\gamma_0 = 20$. Input phase $\phi_0 = 105°$. Injected electrons were uniformly distributed in phase space. The output beam is shifted along the radial axis for clarity in this figure.

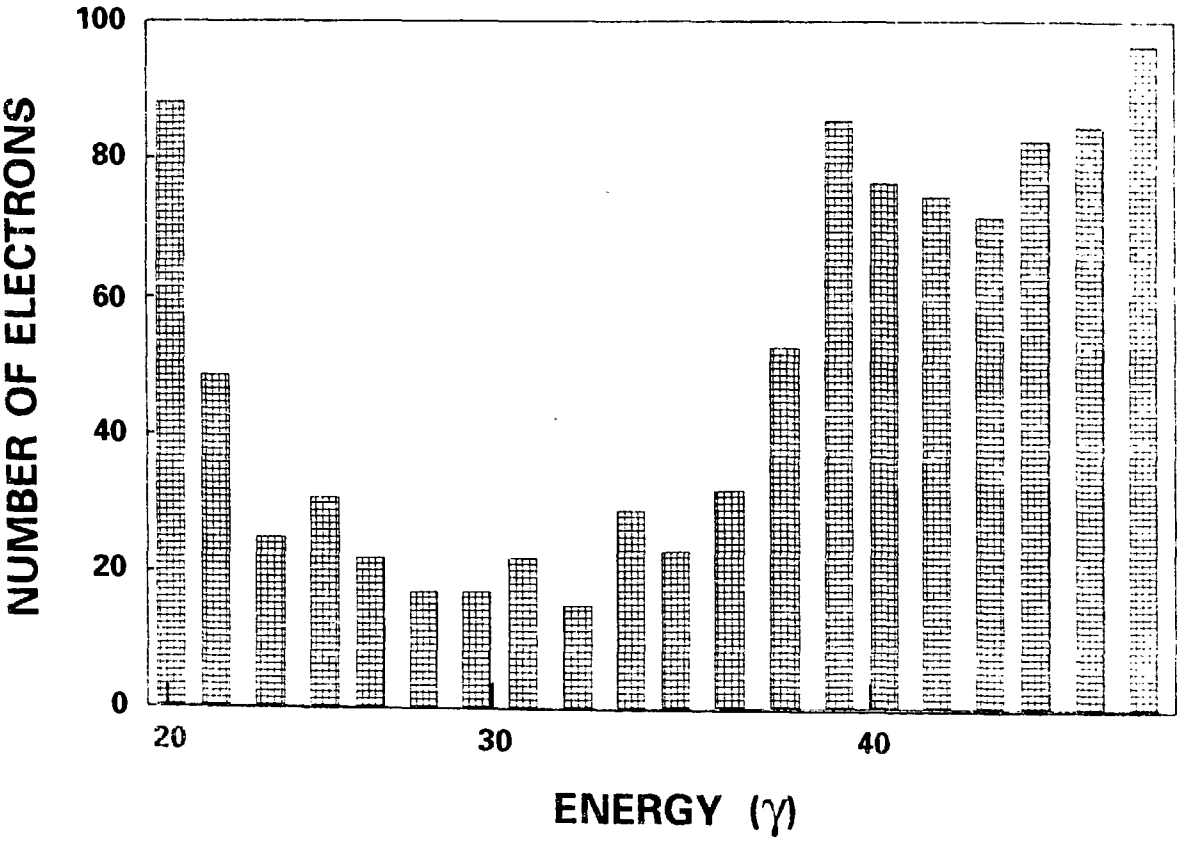

Fig. 22 (b) Accelerated electron energy spectrum for the case shown in Fig. 22 (a).

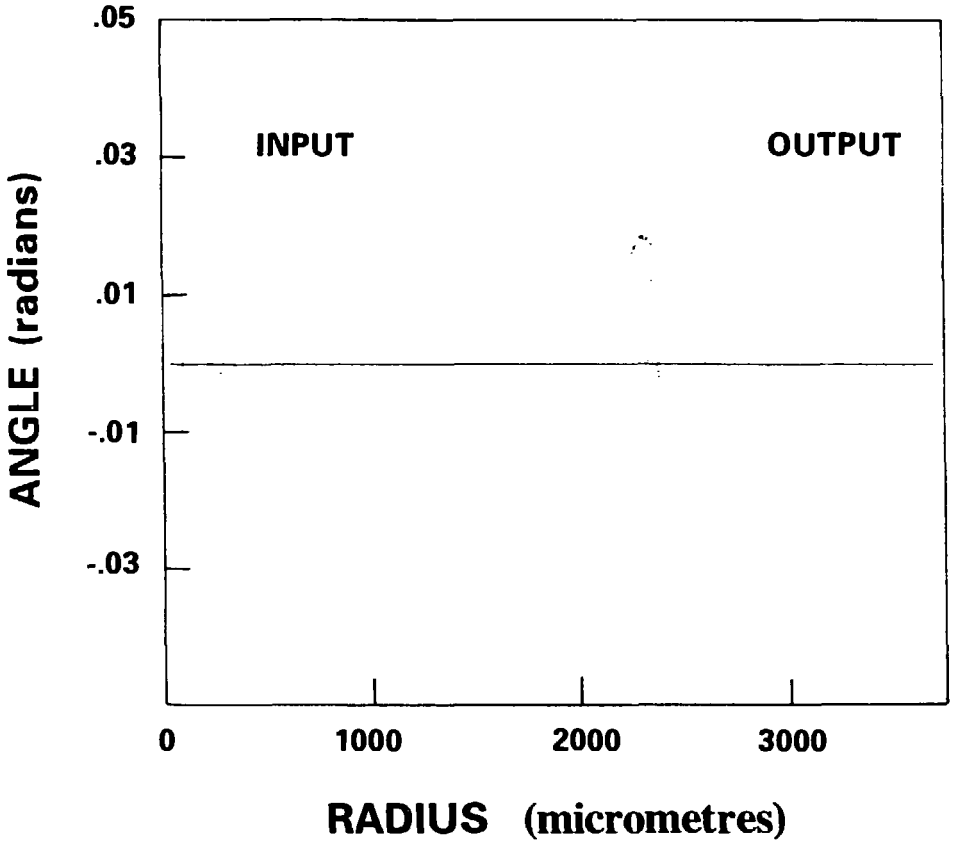

Fig. 23 Radial emittance diagrams at the input (object) and output (image) planes for electrons injected into a two-dimensional plasma wave. Plasma wave amplitude $\epsilon = 0.24$, wave phase velocity $\beta_p = 0.9995$. Injected electron energy $\gamma_0 = 20$. Input phase $\phi_0 = 90°$. Injected electrons were randomly distributed in phase space. The output beam is shifted along the radial axis for clarity in this figure.

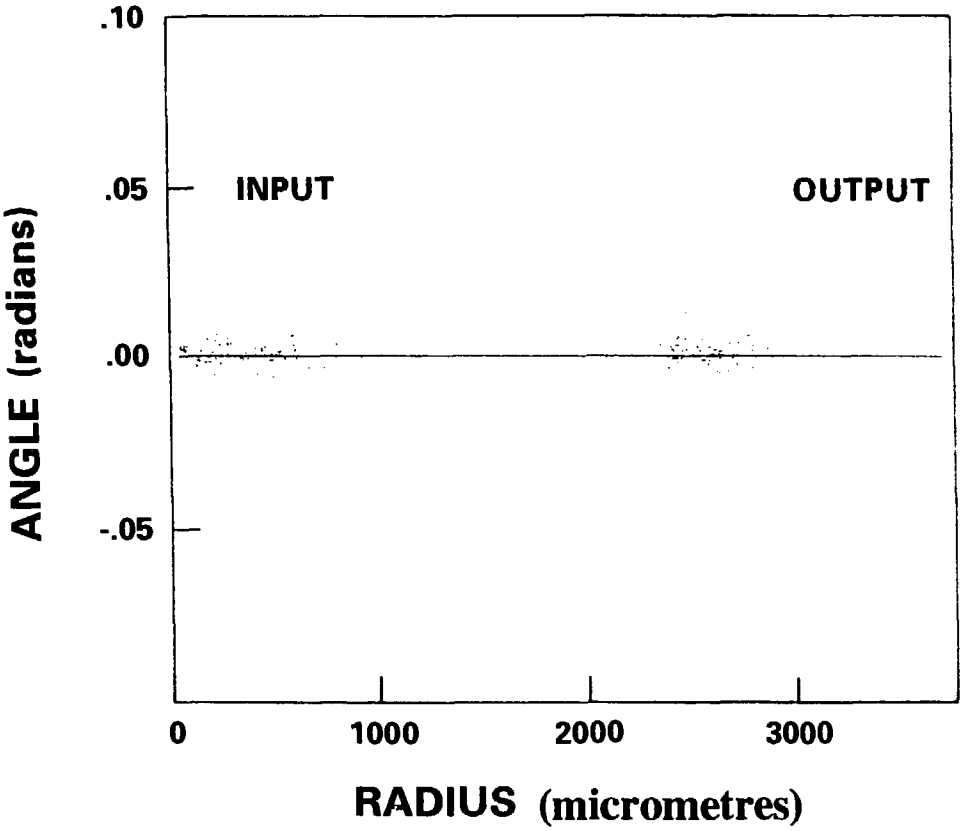

Fig. 24 Radial emittance diagrams at the input (object) and output (image) planes for electrons injected into a two-dimensional plasma wave. Plasma wave amplitude $\epsilon = 0.24$, wave phase velocity $\beta_p = 0.9995$. Injected electron energy $\gamma_0 = 20$. Input phases were uniformly distributed between $\pm \pi$. Injected electrons were randomly distributed in phase space. The output beam is shifted along the radial axis for clarity in this figure.

ISSN 0067-0367

To identify individual documents in the series we have assigned an AECL- number to each.

Please refer to the AECL- number when requesting additional copies of this document

from

Scientific Document Distribution Office
Atomic Energy of Canada Limited
Chalk River, Ontario, Canada
K0J 1J0

Price: B

ISSN 0067-0367

Pour identifier les rapports individuels faisant partie de cette série nous avons assigné un numéro AECL- à chacun.

Veuillez faire mention du numéro AECL- si vous demandez d'autres exemplaires de ce rapport

au

Service de Distribution des Documents Officiels
Énergie atomique du Canada limitée
Chalk River, Ontario, Canada
K0J 1J0

Prix: B

0716-92